Title

Identifying functional ubiquitylation during intracellular bacterial pathogen infection

Permalink

https://escholarship.org/uc/item/1nn9x2cg

Author

Parry, Trevor J.

Publication Date

2015

Peer reviewed|Thesis/dissertation

Identifying functional ubiquitylation during intracellular bacterial
pathogen infection

by

Trevor J. Parry

DISSERTATION

Submitted in partial satisfaction of the requirements for the degree of

DOCTOR OF PHILOSOPHY

in

Biochemistry and Molecular Biology

in the

GRADUATE DIVISION

of the

UNIVERSITY OF CALIFORNIA, SAN FRANCISCO

Copyright 2015

by

Trevor J. Parry

Acknowledgments

I would first like to thank my thesis advisor, Jeff Cox, for accepting me in to his lab, supporting me as I started a new and risky project, and teaching me how to "think big" in science. I would also like to thank him for making my time at UCSF so enjoyable. All of the shared jokes, pitchers of beers, and conversations about how disappointing Cal football was that season have made it a pleasure to work for him.

I next would like to thank all of those who contributed to my project in both major and minor ways. Bennett Penn has been the most influential scientist in my day to day life; always willing to discuss/troubleshoot problems and let me know what controls I'm missing or what other conclusions my data may suggest. I would not be the scientist I am today without him. Sam Bell and Emma Powell have been such great lab mates and friends to me, and I am forever grateful for the time I shared inside and outside lab with them. Eric Chow has contributed so much to this project; teaching me how to perform aerosol infections, prep RNAseq libraries, and has been so generous with his time. Our mass spectrometry collaborators Jeff Johnson, Erik Verschueren, Tasha Johnson, Billy Newton, and Nevan Krogan have been paramount to the success of this project. Thanks to Michael Johnston for his work and helpful advice on the bioinformatics, and to Christina Homer for teaching me everything I know about RNAseq data analysis. I would also like to thank all of the other members of the Cox lab for being supportive, giving much constructive criticism, and always being great coworkers. I would like to thank my thesis committee Anita Sil, Hiten Madhani, and Jeff Cox for their guidance and support of this project.

Lastly, I would like to thank my friends and family. My parents Tom and Julie have always supported me as I have tried to figure out what I am doing in life. My brother Skyler and his wife Angela have been amazing friends and supporters. All of my friends from high school, college, and beyond (who are always ridiculous) have made life so much fun. Most importantly, I would like to thank my wife Stephanie, who has been my biggest supporter, my travel partner, and my co-adventurer through life.

Abstract

Ubiquitin and ubiquitin-like proteins impart regulatory information during innate immune responses to infection, but the scope of their role in coordinating the responses of immune cells to infection is unknown. Recent advances in immmunoaffinity purification of ubiquitylated peptides, paired with high accuracy mass-spectrometry, have provided a new platform to measure global cellular ubiquitylation with extraordinary depth. Here we report the application of this methodology to quantitatively measure changes in ubiquitylation of the macrophage proteome during infection with three intracellular bacterial pathogens: *Mycobacterium tuberculosis*, *Salmonella enterica* serovar Typhimurium, and *Listeria monocytogenes*. This has revealed thousands of ubiquitylation events that occur early after infection, most of which were previously unknown. Unlike transcriptional responses to bacterial infection, which are largely monotonic, our results reveal a surprising diversity in ubiquitin-mediated responses to each pathogen. Likewise, using well-defined attenuated bacterial mutants revealed a remarkable ability of macrophages to discriminate virulent from non-virulent bacteria, suggesting macrophages can integrate information about the nature of the engulfed bacteria and elicit unique responses. Many of these changes likely play functional roles in host resistance, as we have identified a novel ubiquitin-modified pathway, the antiviral OASL1-IRF7 pathway, which is critical for *Mycobacterium tuberculosis* growth *in vitro* and *in vivo*.

Table of contents:

List of tables:

List of figures:

Chapter 3

Chapter 1: Introduction

Mycobacterium tuberculosis, the causative agent of human tuberculosis, currently infects approximately one third of the human population, killing more than 1.5 million people annually (WHO 2014). In 2014, the death toll associated with tuberculosis infection outpaced HIV-related deaths, and 20-33% of all HIV deaths were due to coinfection with *M. tuberculosis* (Getahun et al. 2010, Pawlowski et al. 2012,UNAIDS 2014). Tuberculosis infection is passed from person to person, typically by coughing or sneezing from actively infected carriers (Kaufmann 2001). *M. tuberculosis* is one of the most infectious diseases in the world, and certainly the most infectious bacterial pathogen, with an infectious dose believed to be between one and ten bacilli (Riley et al. 1995). Currently there are four frontline drugs used to treat tuberculosis, but the rates of drug resistance in *M. tuberculosis* are on the rise. It is predicted that 20% of all new *M. tuberculosis* infections are resistant to one or these four drugs, and 5% are resistant to at least two (WHO 2014). The increase in antibiotic resistant strains of *M. tuberculosis* coupled with a population explosion, particularly in underdeveloped countries, necessitates further research into this organism to better understand its lifestyle and interactions with the host during infection.

M. tuberculosis is first taken up by macrophages in the lung where it modulates the host cell to establish a replicative niche conducive to bacterial growth. *M. tuberculosis* harbors a number of complex mechanisms to establish itself in the host and block or mitigate antibacterial responses including the modulation of PI3Kinase signaling to arrest phagosomal maturation (Vergne et al. 2003, Vergne et al. 2005), and increased resistance to acidification (Vandal et al. 2008). Infection of alveolar macrophages induces the expression and secretion of a diverse

number of cytokines and chemokines (Sadek et al. 1998), and promotes the recruitment of other immune cells (macrophages, dendritic cells, etc.) to the area of infection. Infiltration of the site of infection by immune cells induces the formation of granulomas which wall off areas of infection and provide a space for *M. tuberculosis* to grow both intra and extracellularly (Miranda et al. 2012). Ultimately, in actively infected patients, the granulomas burst and release the bacteria, allowing for infection of new hosts.

While the lifecycle of *M. tuberculosis* involves many steps that require complex interactions with the host, the I am interested in the early interactions between *M. tuberculosis* and its target cell, alveolar macrophages, particularly focusing on identifying innate immune pathways used by macrophages to combat *M. tuberculosis* infection (Watson et al. 2012, Manzanillo et al. 2012, Watson et al. 2015). In the last decade, the autophagy pathway has been identified as a new type of innate immunity implicated in the control of a number of intracellular pathogens that access the cytosol (Thurston et al. 2009, Zheng et al. 2009 Cemma et al. 2011), including *M. tuberculosis* (Gutierrez et al. 2004, Ponpuak et al. 2010). A number of components of the machinery that recognize and clear intracellular pathogens by autophagy have been identified, but how cells target cytosolic pathogens for destruction remains unclear.

Autophagy was first described as a nonselective, bulk degradation process of cytoplasmic material in response to starvation (Furuno et al. 1982, Oshita et al. 1986). During starvation, cells wall off portions of their cytoplasm, including whole organelles, into double membrane structures termed autophagosomes. These autophagosomes fuse with the lysosome, leading to the degradation of its cargo in an attempt to recycle metabolites during nutrient limitation (Baba et al. 1994). A large effort to determine the identity and biochemical functions of the core proteins involved in autophagy has revealed more than 30 proteins implicated in this process in

eukaryotic cells. Importantly, yeast Atg8 (and the mammalian homologue LC3) was shown to be an essential protein for autophagy that localizes to the autophagosome, and has proven to be a useful marker for autophagosome biogenesis (Kebaya et al. 2000).

In recent years our understanding of the role of autophagy in eukaryotic cell biology has expanded, identifying autophagy as a process that can selectively target specific cytoplasmic content for degradation by the lysosome (Sha et al. 2010, Lee et al. 2010). Key steps in targeting by selective autophagy include the accumulation of ubiquitin around the target, the binding of ubiquitin by the adaptor proteins p62 and NDP52, which in turn recruit LC3 to initiate autophagosome formation. This selective autophagy pathway has been shown to be critical in the clearance of protein aggregates, damaged organelles, and of particular interest to our lab, intracellular pathogens including *Mycobacterium tuberculosis* (Olzmann et al. 2007, Narendra et al. 2008).

During the early stages of infection, macrophages phagocytose *M. tuberculosis*, and the bacterium maintains itself inside an early endosome-like compartment (Russell. 2001) through the secretion of effector proteins by the specialized type VII secretion system, ESX-1 (MacGurn and Cox. 2007). *Mycobacterium tuberculosis* and the related pathogenic species *Mycobacterium marinum* have both been shown to be targeted by selective autophagy for degradation in macrophages, and this is dependent upon the pathogens accessing the cytoplasm using their type VII secretion systems (Gutierrez et al. 2004, Lerena and Colombo. 2011). Though it has been shown that ubiquitin accumulates around intracellular pathogens during the initial stages of selective autophagy, the ubiquitylated substrates, and the E3 ubiquitin ligases involved, remain a mystery (Perrin et al. 2004). Parkin, an E3 ligase involved in the ubiquitylation of damaged mitochondria, is required for the accumulation of ubiquitin around *Mycobacterium tuberculosis*

(Manzanillo et al. 2013). It is unclear, however, if host or bacterial proteins are ubiquitylated, and if Parkin is directly or indirectly responsible for the ubiquitylation.

It was recently shown that the ubiquitin that accumulated around *M. marinum* during macrophage infection was a mixture of both K48 and K63-linked ubiquitin, but it was unclear how these linkages were associated with the invading bacteria (Collins et al. 2009). Our lab has observed this mixed linkage accumulate around *M. tuberculosis* as well (Watson et al. 2012). While ubiquitin has been known to play a critical role during early detection of invading bacterial pathogens, the targets of ubiquitin in host cells has not been well characterized. This has been due in large part to the lack of tools sufficient to quantitatively measure global ubiquitylation of the host proteome during infection. A better understanding of the targets of ubiquitylation during infection with a panel of intracellular bacterial pathogens is needed, and has proven to be an area of active investigation.

Chapter 2: Identifying functional ubiquitylation during intracellular bacterial pathogen infection

Abstract:

Ubiquitin and ubiquitin-like proteins impart regulatory information during innate immune responses to infection (Zinngrebe et al. 2014), but the scope of their role in coordinating the responses of immune cells to infection is unknown. Recent advances in immmunoaffinity purification of ubiquitylated peptides, paired with high accuracy mass-spectrometry, have provided a new platform to measure global cellular ubiquitylation with extraordinary depth (Ordureau et al. 2015). Here we report the application of this methodology to quantitatively measure changes in ubiquitylation of the macrophage proteome during infection with three intracellular bacterial pathogens: *Mycobacterium tuberculosis*, *Salmonella enterica* serovar Typhimurium, and *Listeria monocytogenes*. This has revealed thousands of ubiquitylation events that occur early after infection, most of which were previously unknown. Unlike transcriptional responses to bacterial infection, which are largely monotonic (Iwasaki and Medzhitov, 2015), our results reveal a surprising diversity in ubiquitin-mediated responses to each pathogen. Likewise, using well-defined attenuated bacterial mutants revealed a remarkable ability of macrophages to discriminate virulent from non-virulent bacteria, suggesting macrophages can integrate information about the nature of the engulfed bacteria and elicit unique responses. Many of these changes likely play functional roles in host resistance, as we have identified a novel

ubiquitin-modified pathway, the antiviral OASL1-IRF7 pathway, which is critical for

Mycobacterium tuberculosis growth *in vitro* and *in vivo*.

Introduction:

The initial interactions between pathogens and innate immune cells has been described primarily by the transcriptional networks that coordinate pro-inflammatory responses to conserved microbial products. These initial transcriptional responses to infection are rapid but largely generic (Leber et al. 2008, Manzanillo et al. 2012) – vastly different microbes (e.g. viruses and bacteria) give rise to qualitatively similar responses via activation of a broad array of receptors linked to a limited set of transcriptional regulators (Mogenson 2009, Vance et al. 2009, Janeway and Medzhitov, 2002). According to this paradigm, the complexity of information available, for example gram-negative vs. gram-positive bacterial pathogens, is reduced into monotonic activation of pro-inflammatory signaling pathways. How tonic signals generated at the earliest stages of infection shape the nature of the specific immune responses tailored to the invader is not well understood. A prevailing model is that specificity in innate immune responses is achieved by orchestrated secondary interactions with other innate cells recruited to the infection focus (Iwasaki and Medzhitov, 2015). However, a growing literature suggests that macrophages and dendritic cells can actively participate in shaping specific immune responses in a cell-autonomous fashion, especially the discrimination of pathogens versus non-pathogens, at the very earliest stages of infection (Huang et al. 2002, Bohsali et al. 2010).

While global gene expression platforms have been used to comprehensively probe the initial macrophage responses to infection, the role of post-translational modifications (PTM) of proteins, which regulate virtually every cellular process, in this response is poorly understood.

Modification of host proteins with ubiquitin (and ubiquitin-like molecules such as ISG-15) has been demonstrated to play important regulatory functions in innate immunity, with roles in signaling, vesicular trafficking, and targeting of intracellular pathogens to the autophagy pathway (Perrin et al. 2004, Zinngrebe et al. 2014, Davis and Gack 2015, Angot et al. 2007). Indeed, some pathogens have evolved pathogenic strategies to manipulate the ubiquitin system, including HIV, which hijacks ubiquitylation machinery to control host cell responses (Jager et al. 2011), and *Salmonella enterica* serovar Typhimurium , which targets ubiquitin pathways by secretion of effector proteins into host cells (Narayanan and Edellman 2014). Unfortunately, a comprehensive view of the ubiquitylation changes during innate immune responses has been limited by a lack of facile tools to study these modifications in a global fashion. Previous studies have utilized overexpression of epitope-tagged ubiquitin followed by immunoprecipitation and mass spectrometry (MS) identification to qualitatively identify ubiquitylated host proteins during bacterial infection of macrophages (Ivanov and Roy 2013), but this methodology is limited by sensitivity issues and problematic quantification schemes. Recent technical advancements in proteomics have enabled a methodology, termed di-glycine ubiquitin-remnant mass spectrometry (diGly-MS) that quantitatively measures endogenous ubiquitylation giving lysine-site resolution across the entire proteome of a cell (Kim et al. 2011, Sarraf et al. 2013, Udeshi et al. 2013). We have applied this technology to measure, for the first time, global ubiquitylation dynamics induced by infection of multiple intracellular bacterial pathogens, and well-defined attenuated mutants, in macrophages at early time points during infection. While these studies have identified a set of stereotypical "core" ubiquitylation changes of host proteins, they have revealed a surprising level of uniqueness in ubiquitylation changes in response to different bacterial pathogens. Our data suggest that this level of specificity is influenced not only by differences in

the nature of the bacterial structures, but also reflective of the unique pathogenic strategies of each pathogen. This approach has led to the identification of an ubiquitin-modified pathway that is critical for growth of *Mycobacterium tuberculosis* in its host.

Results:

To quantitatively measure ubiquitylation changes during macrophage infection, we used stable isotope labeling by amino acids in cell culture (SILAC) to label RAW 264.7 macrophages, and infected these monolayers with three intracellular bacterial pathogens: *Listeria monocytogenes*, *Salmonella enterica* serovar Typhimurium (hereafter referred to as *S. typhimurium*), and *Mycobacterium tuberculosis*. These pathogens were chosen as they represent the three major classes of bacteria (gram-positive, gram-negative and acid-fast) and utilize contrasting pathogenic strategies to replicate inside macrophages. Ubiquitylation of host proteins was quantified at two hours post infection for both *L. monocytogenes* and *S. typhimurium* infections, and six hours post infection for *M. tuberculosis* infection, as these time points represent the peak of ubiquitylation observed around these pathogens in this cell type (Birgmingham et al. 2006, Lam et al. 2013, Watson et al. 2012). Proteins were extracted from the infected monolayers, digested with trypsin, and peptides with ubiquitin remnants were purified by immunoaffinity enrichment and identified using quantitative high-resolution mass spectrometry (figure 2.1). Infection-induced changes in ubiquitylation were quantified relative to mock-infected cells, and our data analysis excluded all ubiquitylated peptides that are not detected in both biological replicates. We quantitatively measured the ubiquitylation of 5,579 unique lysine residues on 1,807 proteins during infection with wild-type *L. monocytogenes*, 4,452 unique lysine residues on 1,560 proteins during infection with wild-type *S. typhimurium*, and 5,612 unique lysine residues on 1,839 proteins during wild-type *M. tuberculosis* infection.

We analyzed the combined set of biological replicates with an in-house computational pipeline, built around the MSstats bioconductor package, to determine the set of proteins with significant changes (p<0.05 and fold change ≥ 2 relative to mock infected) in ubiquitylation. We mapped and clustered all of the ubiquitylation sites that were detected during all three infections (and considered significant in at least one infection) with the expectation that there would be a similar stereotypical ubiquitylation response similar to what is seen at the transcriptional level (figure 2.2a and b). There are six lysine residues that are ubiquitylated during infection with all three pathogens: K88 of CXCL2, K66 and K131 of TNFAIP3, K127 of MYD88, K501 of PDCD6IP, and K170 of PELLINO1. Additionally, we averaged the fold ubiquitylation change for every lysine residue across each identified protein, and clustered significant ubiquitin changes on entire proteins for all three infections (figure 2.3a and b). Surprisingly, infection with the three wild-type strains gave rise to unique patterns of ubiquitylation, with only a small subset of shared or "core" ubiquitylation events amongst the three infections. Interestingly, the ubiquitylation patterns elicited by *S. typhimurium* and *M. tuberculosis*, pathogens that remain associated with phagosomal membranes, clustered more closely with one another than either did with *L. monocytogenes*, which ruptures phagosomes and moves within the cytosol. These two infections gave rise to a number of common changes, potentially representing a core set of lysine sites that are ubiquitylated when cells detect vacuolar-residing organisms.

For each pathogen, we used DAVID (Huang et al. 2009) to cluster all of the significant proteins into functional categories based on gene ontology-term analysis in order to identify both pathogen-specific and common processes that are ubiquitylated during each infection (figure 2.4). These categories represent the functional groups or processes that are disproportionately represented in our dataset relative to the entire proteome for *M. tuberculosis* infection (table 1),

L. monocytogenes infection (table 2), and *S. typhimurium* infection (table 3). While some

categories are enriched in all three infections, such as trafficking proteins and nucleotide

metabolism, and likely represent general host responses to infection, other categories are unique

to specific bacterial infections. In particular, ubiquitylation of mitochondrial and lysosomal

proteins is significantly enriched during *M. tuberculosis* infection whereas proteins that localize

to the ER or are involved in translation are specifically enriched in *L. monocytogenes* infection.

Cell death proteins are enriched during both *L. monocytogenes* and *M. tuberculosis* infection, but

not *S. typhimurium* infection. Overall, fewer proteins clustered into significantly enriched

categories during *S. typhimurium* infection, consistent with the notion that this pathogen modifies

the ubiquitin system extensively.

Macrophages can discriminate pathogens from non-pathogens by assessing phagosome

damage as a proxy for virulence (Randow et al. 2013). This is achieved by monitoring

phagosome membrane integrity via engagement of receptors that recognize either bacterial

"patterns" in the cytosol or lumen, and trigger inflammatory transcriptional responses, termed the

cytosolic response (Thurston et al. 2012, Vance et al. 2009). To determine if similar changes are

manifest at the level of ubiquitylation, we performed the exact same di-Gly experiments using

well-defined bacterial mutants deficient in major virulence determinants that damage phagosome

membranes. Similar numbers of ubiquitylated lysine residues and proteins were identified in

each mutant infection compared to its wild-type counterpart (5,563 sites on 1,808 proteins for

Δ*hly L. monocytogenes*, 4,313 sites on 1,525 proteins for Δ*ssav*Δ*orga S. typhimurium*, 5,546 sites

on 1,828 proteins for Δ*eccd M. tuberculosis*) and significant ubiquitylation sites were identified

for each mutant as described above. Interestingly, while infection of macrophages by wild-type

L. monocytogenes induces the most robust ubiquitylation we observe, deletion of the pore-

forming toxin LLO reduces the number of significantly ubiquitylated lysine residues from 1,134

to 128 (figure 2.5a). The LLO mutant *L. monocytogenes* is completely attenuated (Glomski et al.

2003), and we consider this mutant to be the equivalent of a non-pathogenic bacterium. Thus, the

few lysine residues that are ubiquitylated during infection with the LLO mutant are likely those

that are ubiquitylated in response to the phagocytosis of non-pathogens. The SpiI/II double

knock out *S. typhimurium* infection results in a greater change in ubiquitylation of the host

proteome than wild-type infection (figure 2.5b). *S. typhimurium* is known to secrete

deubiquitinases that modify the post-translational modification state of the host proteome

(Mesquita et al. 2012), and it is likely that some or many of the lysine residues who's

ubiquitylation increases during infection with the type III secretion deficient bacteria are targets

of these secreted deubiquitinases. While the type VII secretion deficient *M. tuberculosis* is

attenuated relative to the wild-type strain, it is still able to grow in mice (Stanley et al. 2003), and

we consider it to be the least attenuated of the three mutant strains tested. It is then unsurprising

that the ESX1 mutant *M. tuberculosis* has the most similar ubiquitylation fingerprint (relative to

its wild-type counterpart) when compared to the other wild-type/mutant pairs tested here (figure

2.5c).

To identify ubiquitin-modified pathways that are functionally important, we selected 41

highly ubiquitylated proteins during *M. tuberculosis* infection, which included both "core"

ubiquitylated proteins and those with *M. tuberculosis*-specific changes. We stably overexpressed

each protein individually in the murine macrophage-like J774 cell line and infected each stable

cell line with a strain of *M. tuberculosis* constitutively expressing a codon-optimized

LuxBCADE operon (Kampmann et al. 2000, Schiebler et al. 2014). We tracked bacterial growth

by measuring luminescence every 24 hours over a five-day time course and monitored

11

macrophage survival by assessing monolayer integrity at each time point. Of the 41 host genes, two gave rise to poor macrophage growth upon overexpression and were eliminated from the screen. Of the remaining 39 genes, nine gave rise to interesting phenotypes after infection (table 4 and the following representative experiments): OASL1 and PELLINO1 led to decreased bacterial replication (figure 2.6a and b), VAMP8 gave rise to increased *M. tuberculosis* replication (figure 2.6b), and CD14 and ZDHHC20 led to rapid macrophage lysis specifically after infection (figure 2.7a and b). In line with our findings during *M. tuberculosis* infection, PELLINO1 was recently described to be involved in activation of a number of pro-inflammatory pathways known to play a role in protection against *Mycobacterial* infection (Murphy et al. 2015). Additionally, CD14 has recently been described to activate necrosis in alveolar macrophages after engagement with LPS (Daqvadori et al. 2015). While neither one of these publications involved *M. tuberculosis* infection, their conclusions fit the models predicted by our experiments, and thus validate our screening approach.

We selected OASL1, a protein recently identified as playing a critical role in the response to viral infection (Lee et al. 2013), for further study as it gave rise to the strongest and most reproducible phenotype. Bacterial repression was specific to OASL1, as similar overexpression of either GFP or another highly ubiquitylated protein identified in the di-Gly dataset, Renin Receptor, had no effect on bacterial survival (figure 2.6a). The observed difference in bacterial growth was not an artifact of premature macrophage death, as OASL1 expressing macrophages survived longer than their GFP-expressing counterparts during infection, and rates of phagocytosis were identical. Interestingly, while OASL1 is also ubiquitylated during *S. typhimurium* infection, over-expression of OASL1 had no effect on *S. typhimurium* growth in macrophages. OASL1 protein levels decreased approximately two fold at six hours post-

infection in bone marrow-derived macrophages (figure 2.8a) even though OasL1 transcript levels are approximately eight fold higher at this time point (figure 2.8b), suggesting that ubiquitylation of OASL1 leads to its degradation. OASL1 is a translation repressor of approximately 145 genes, many of which are involved in type-1 interferon, a pathway activated by *M. tuberculosis* during infection (Teles et al. 2013). As expected, decreasing levels of OASL1 in infected macrophages leads to a concomitant increase the OASL1-target IRF7 protein levels (figure 2.8c). We next tested whether OASL1 colocalizes to the bacteria during infection, as the repressive effect of OASL1 may be due to direct interaction with the pathogen, but no colocalization was detected (figure 2.9a and b). To determine whether the repressive effect of OASL1 was due to the translational repression of one or more of its targets, we made a three amino acid substitution in OASL1 (R192E, K196E, and K201E), termed OASL1-RKK, that reduces its ability to bind its target RNAs (Lee et al. 2013). Expression of OASL1-RKK allowed greater bacterial growth than wild-type OASL1 (figure 2.10), suggesting that the effect of OASL1 on bacterial growth is due to translational repression of one or more of its target transcripts. We also tested whether lysine 327 (the lysine residue ubiquitylated during *M. tuberculosis* and *S. typhimurium* infection) was required for the repressive effect on *M. tuberculosis* growth by making a K327R substitution. J774 cells overexpressing wild-type of K327R OASL1 were equally resistant to *M. tuberculosis* growth (figure 2.11).

The OASL1 target of immediate interest to us that may account for the observed growth defect was Interferon Regulatory Factor 7 (IRF7), a transcription factor that is important for sustained type-1 interferon signaling during viral infection (Daffis et al. 2008). If the observed defect in bacterial growth is due to OASL1's repression of Irf7, we would expect that decreasing levels of IRF7 would phenocopy over-expression of OASL1. Macrophages stably expressing two

different Irf7 shRNAs were resistant to bacterial growth relative to control cells (figure 2.12a and b). To confirm that OASL1 over-expression suppresses bacterial growth exclusively through its effect on IRF7 levels, we co-expressed GFP or IRF7 constructs including its 5' UTR with or without the OASL1 binding site in J774 cells expressing OASL1. No difference was detected in *M. tuberculosis* growth in the cells expressing GFP or an OASL1-sensitive IRF7, but growth was restored in cells expressing an OASL1-insensitive IRF7 (figure 2.13a). As expected, 40% more IRF7 protein is made in macrophages expressing the OASL1-insensitive IRF7 relative to the OASL1-sensitive construct (figure 2.13b). Knockdown of OasL1 (figure 2.14a and b) had no consistent effect on bacterial growth. One stably selected shRNA allowed more bacterial growth than control cells while the other shRNA repressed bacterial growth. To clarify this result, we sought to overexpress IRF7 in J774 cells (this should be the same effect as knocking down OasL1). Overexpression of IRF7 (figure 2.15) had no effect on *M. tuberculosis* growth in J774 macrophages, suggesting that the endogenous IRF7 is sufficient to elicit robust bacterial growth, while increasing IRF7 expression by either knocking down OasL1 or exogenously overexpressing IRF7 has no additional benefit.

Importantly, bone marrow-derived macrophages elicited from Irf7$^{-/-}$ knockout mice were highly resistant to *M. tuberculosis* growth (figure 2.16). There are two well characterized pathways in macrophages that efficiently kill *M. tuberculosis*: trafficking to the lysosome through the autophagy pathway (Watson et al. 2012), and direct bacterial killing by the production of nitric oxide (Kwon 1997, Macmicking et al. 1997). We first tested whether there was increased trafficking of the bacteria to the lysosome in the Irf7$^{-/-}$ knockout bone marrow-derived macrophages. Colocalization of the bacteria with the late endosome/lysosome marker ATP6E was the same at days one, three, and five post-infection wild-type and Irf7$^{-/-}$ knockout

macrophages (figure 2.17a and b). Next, we measured nitric oxide production in wild-type and Irf7^{-/-} knockout macrophages at days one and three post-infection. While neither cell type elicits high levels of nitric oxide, as production increases dramatically only after interferon gamma stimulation (Blanchette et al. 2003) which is absent in our macrophage luciferase assay, the levels produced by wild-type and knockout cells are comparable (figure 2.18).

The transcriptional regulon of IRF7 has yet to be adequately described during bacterial infection, and it is likely that one or more of the transcriptional targets of IRF7 are the cause of the repressive environment in the knockout cells. To begin to understand the transcriptional network regulated by IRF7, we performed RNAseq on mock infected, 24 hour infected, and 72 hour infected wild-type and Irf7^{-/-} knockout bone marrow-derived macrophages in duplicate. At 24 hours post-infection we quantified the transcriptional changes in each cell type relative to the appropriate mock infected control (figure 2.19a). We first identified a number of genes known to be important for responding to *M. tuberculosis* infection including Nos2, IL1α, IL1ß, IL12, and Ifnß (figure 2.19b). There were no strong differences observed in the regulation of any of these genes. Because of the well described role of IRF7 in the regulation of Interferon α signaling, we also looked at the levels of all of the Interferon α genes, but there is no difference between wild-type and knockout cells (surprisingly, Interferon α is not induced at all during macrophage infection with *M. tuberculosis*). We performed a similar comparison of infected cells at 72 hours post-infection (figure 2.20a), a time point when we begin to see a difference in *M. tuberculosis* abundance, but no differences were observed in any of the pro-inflammatory/signaling genes we looked at (figure 2.20b). We next used CuffDiff of the Tophat suite of RNAseq analysis tools to identify the genes that are differentially regulated in these two cell types and found a total of 69 genes that are regulated by IRF7, 57 of which are activated and

15

12 of which are repressed by IRF7 (table 5). We have begun a screen to identify the genes that contribute to the repressive environment of the Irf7$^{-/-}$ knockout macrophages (table 5, in yellow). Briefly, we are individually overexpressing the 57 genes that are upregulated by IRF7 in the Irf7 knockdown J774 cells looking for a rescue of *M. tuberculosis* growth using our luciferase reporter system. In one representative experiment, we have overexpressed GFP and IRF7 in the knockdown cells as our negative and positive controls, respectively, and overexpressed two transcriptional targets of IRF7, AEN and H2-M2 (figure 2.21). Overexpression of H2-M2 has no effect on bacterial growth while overexpression of AEN partially rescues the growth defect of the bacteria in the Irf7 knockdown cells. We have screened through 20 of the targets and found 6 that have a partial rescue phenotype: ACPP, AEN, GBP5, GM14446, MET, and SLC35G2.

We are also interested in identifying the protein-protein interactions between OASL1 and its partners during infection, with particular emphasis on trying to identify any E3 ubiquitin ligases that interact with OASL1. We initially tried to identify these interactors by affinity purification/mass spectrometry, but did not identify anything that was not also detected in our negative controls. We are now adapting a new method of protein-protein interaction, termed BioID, to identify OASL1 interactors in macrophages with and without bacterial infection. This method uses a fusion protein of OASL1 with a mutant BirA domain from *E. coli* which biotinylates lysine residues of proteins that come in to close proximity to our fusion protein (Lambert et al. 2015). We first tested whether expression of a BirA fusion GFP and OASL1 can be stably expressed in RAW 264.7 macrophages (figure 2.22a). While expression of the GFP fusion is approximately seven and a half fold higher than the OASL1 fusion, we can still express the OASL1 at detectable levels. We next tested whether expression of the BirA fusion proteins led to biotinylation of substrates in macrophages. Macrophages were incubated with excess

biotin in the media for 24 hours, and biotinylation was visualized by blotting cell lysates with dye-labelled streptavidin (figure 2.22b). An increase in biotinylation is observed in the cells expressing the BirA-OASL1 fusion (relative to the OASL1 overexpressing cells lacking BirA), and the observed biotinylation is expression dependent, as much higher levels of biotinylation are observed in the BirA-GFP expressing cells. We have now performed biotinylation/biotinylated substrate purification in quadruplicate in BirA-GFP and BirA-OASL1 expressing macrophages with and without *M. tuberculosis* infection. These samples have been submitted for peptide identification by mass spectrometry, and we await the results.

Lastly, to test whether IRF7 plays a role *in vivo* during *M. tuberculosis* infection, we infected wild-type and Irf7$^{-/-}$ C57BL/6 mice via the aerosol route and assayed bacterial growth and determined time to death in these mice. Mice lacking IRF7 were resistant to bacterial growth in both the lungs (figure 2.23a) and spleen (figure 2.23b), and survived challenge longer than their wild-type counterparts (figure 2.23c).

Discussion:

Here we have quantitatively measured the ubiquitylation of the macrophage proteome during multiple intracellular bacterial pathogen infections. To our surprise, while there are a small number of ubiquitylation events shared amongst two or three infections, a huge majority of ubiquitylation was specific to each pathogen. This unexpected result suggests that while bacterial infection may lead to a stereotypical transcriptional output in the host, sensing and ubiquitylation signaling induced by each pathogen is distinct. The difference in ubiquitylation induced by each pathogen likely results both from the unique physiology of each pathogen (gram positive vs. gram negative), as well as the lifestyle of the organism in the host (cytoplasmic vs. vacuolar). It

will be interesting to see how macrophages respond to structurally similar pathogens (e.g. *Salmonella typhimurium* vs. *Legionella pneumophila*) and pathogenic vs. non-pathogenic strains of the same organism (like clinical *E. coli* strains). It will also be interesting to study the differences in ubiquitylation induced by other secretion-competent vs. deficient bacteria. diGly-MS has proven to be a powerful platform for discovery of new host-pathogen interactions and this strategy can be adopted using various bacterial and host cell mutants to further refine our understanding of the role of ubiquitylation in microbial pathogenesis.

Our quantitative ubiquitylation analysis has led to the discovery of an ubiquitin-modified pathway previously unknown to play a role during *M. tuberculosis* infection (figure 2.24). While we do not yet fully understand how bacterial growth suppression is achieved in the Irf7$^{-/-}$ knockout cells and mice, it appears to function through a novel pathway distinct from known mechanisms of the innate immune response to *M. tuberculosis* infection. When examining the transcriptional targets of IRF7 during bacterial infection, it is clear that immune response genes are enriched in our target list. How cells lacking these genes are less permissive to bacterial replication remains a mystery, and overexpression of the initial hits from our secondary screen of IRF7 targets that allows a partial growth rescue (ACPP, AEN, GBP5, GM14446, MET, and SLC3562) do not shed light on this. Recently, IRF7 was described to play a role in obesity and the onset of type II diabetes in mice (Wang et al. 2013). While it is not obvious from our RNAseq data, the bacteria living inside the Irf7$^{-/-}$ knockout cells may not be receiving the nutrients required for proper growth given the recently described role of IRF7 in metabolism. Additionally, these bacteria may not be receiving the appropriate cues that tell them they are in a host cell and should replicate, much like what is seen in *Salmonella* infection in mice lacking

multiple TLRs (Sivick et al. 2014). Further work is required to dissect the pathway(s) that are interrupted in the Irf7^{-/-} cells and mice that are giving us the observed phenotype.

Lastly, OasL1 is just one of the thousands of proteins that are ubiquitylated early during infection, and there are many other proteins that are ubiquitylated early during infection that give rise to observable phenotypes during *M. tuberculosis* infection *in vitro*. The next step will be to quantitatively measure changes in ubiquitylation over a time course of infection, giving us a better picture of the way in which macrophages respond and shape their proteomes over the course of infection. Importantly, we need to also perform these experiments in the presence of a proteasome inhibitor (like MG132) to give better clarity on how the observed ubiquitylation affects a given target (whether ubiquitylation is involved in signaling or protein turnover). It will also be important to look at the role of ubiquitylation in primary cells, as these cells most closely resemble the environment encountered by *M. tuberculosis* in naïve mice. This study represents the first step in understanding ubiquitin in the context of intracellular bacterial pathogen infection.

Figure 2.1

a

"Heavy"
Lys-^{13}C
Arg-^{13}C,^{15}N

"Light"

Ub

mixed
protein
lysate

trypsin
digest

GG

GG

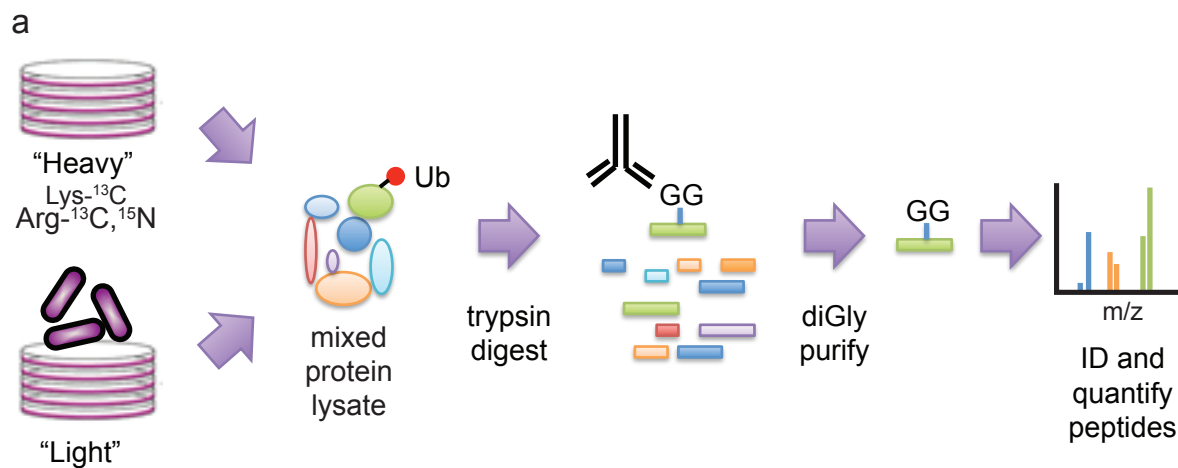diGly
purify

m/z

ID and
quantify
peptides

Figure 2.1: Experimental approach to identifying ubiquitylation of macrophages during infection.

(A) Schematic of the ubiquitin remnant immunoaffinity enrichment protocol to identify ubiquitylated substrates during bacterial infection.
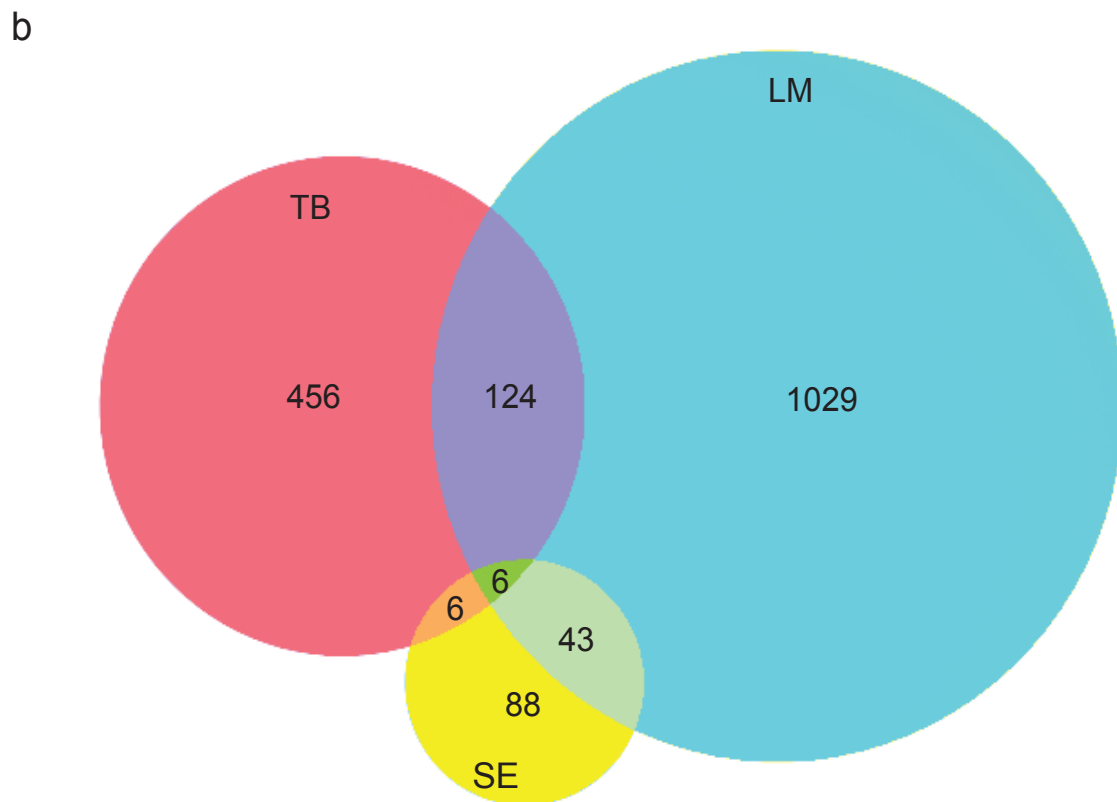
Figure 2.2

a

b

Figure 2.2: Ubiquitylation of lysine residues observed during infection.

(A) Heat map of the average log2 fold change in ubiquitylation for each lysine site detected in all three bacterial infections that was significant (≥two-fold change relative to mock infection, p<0.05) in at least one infection.

(B) Venn diagram representing distinct and shared lysine residues that are significantly ubiquitylated (≥two-fold change relative to mock infection, p<0.05) during bacterial infection.

Figure 2.3

a

b

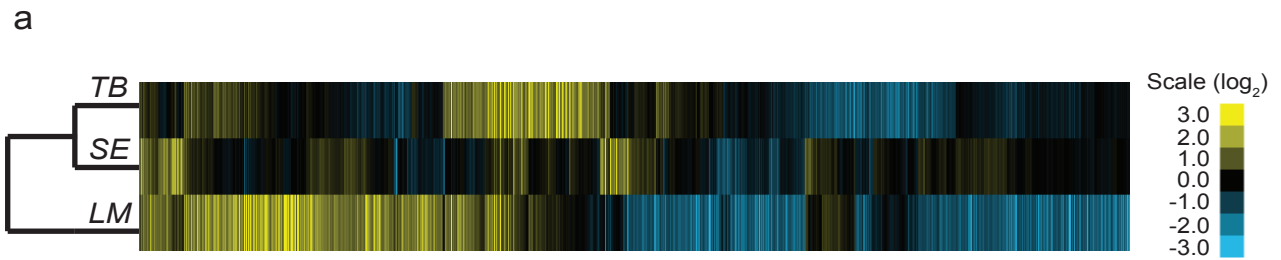**Figure 2.3: Average ubiquitylation of proteins observed during infection.**

(A) Heat map of the average log2 fold change in ubiquitylation for every protein detected in all three bacterial infections that was significant ($\geq$two-fold change relative to mock infection, $p < 0.05$) in at least one infection.

(B) Venn diagram representing distinct and shared proteins that are significantly ubiquitylated ($\geq$two-fold change relative to mock infection, $p < 0.05$) during bacterial infection.
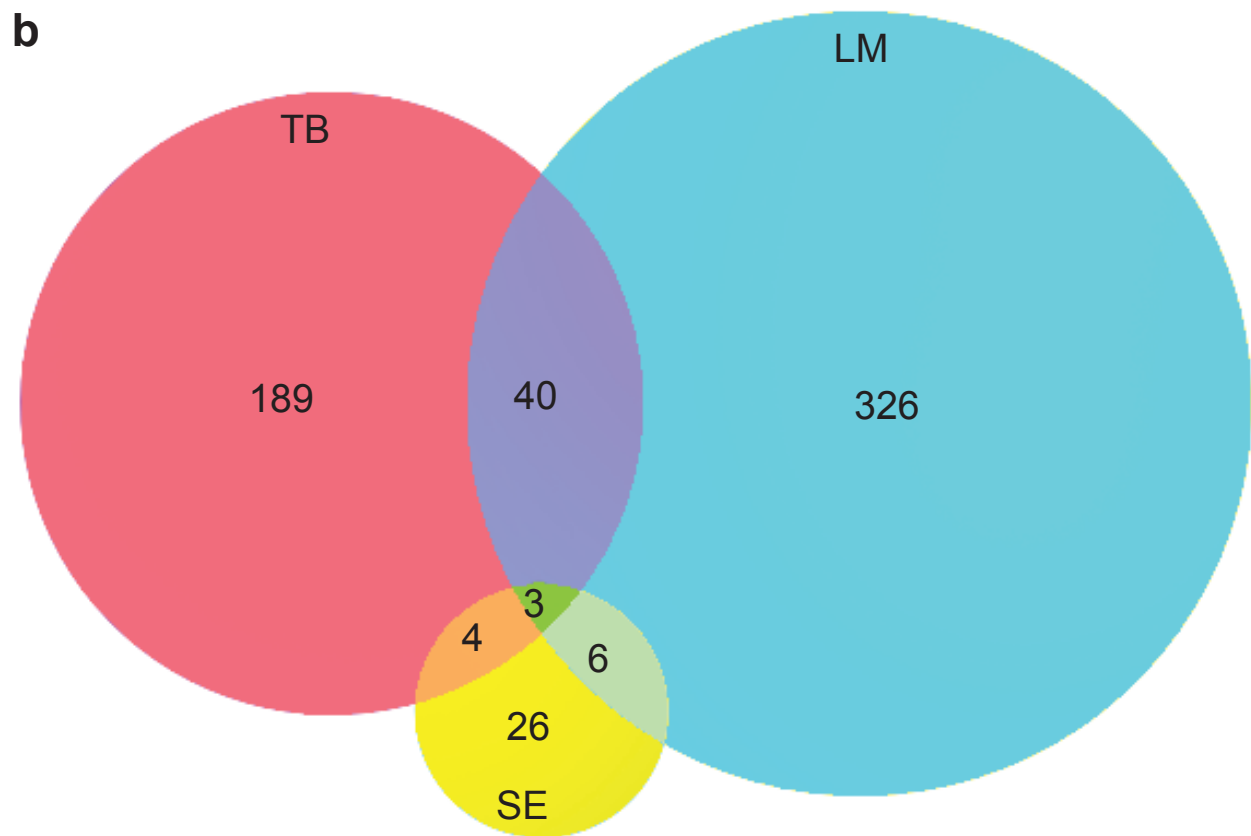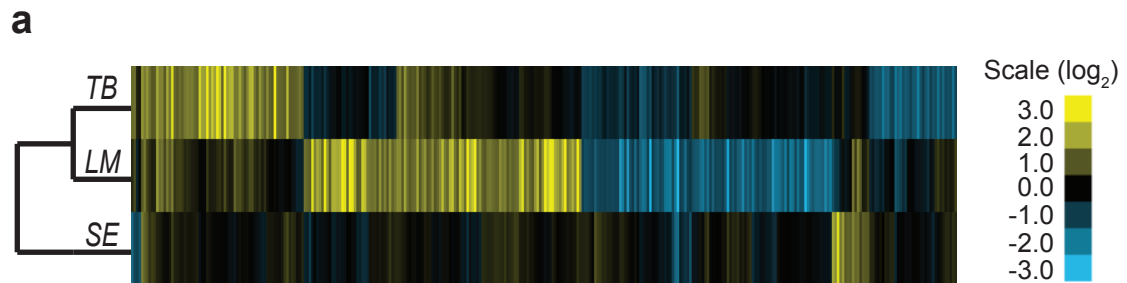
Figure 2.4

a

M. tuberculosis infection

b

L. monocytogenes infection

c

S. typhimurium infection

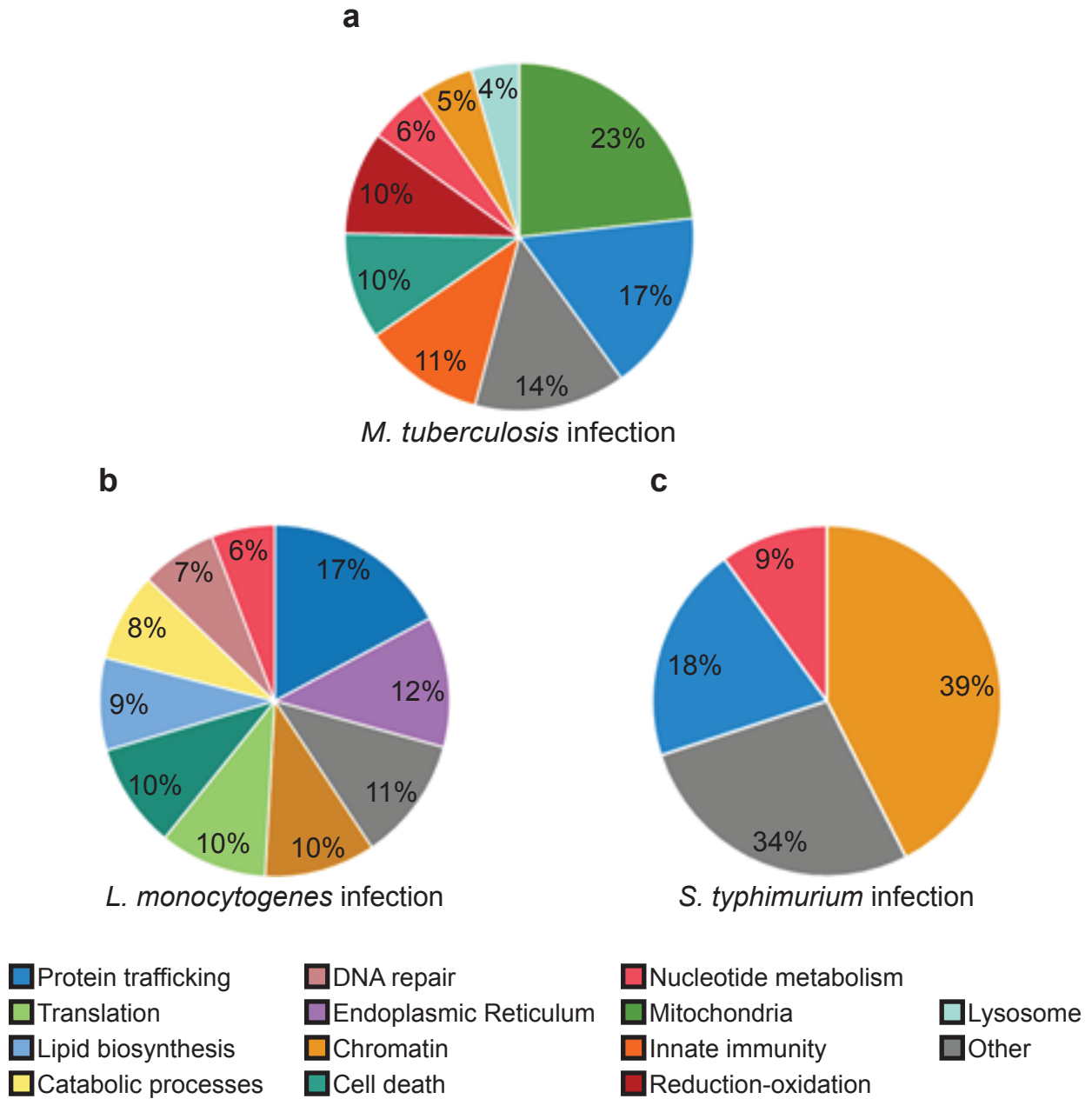|		
■ Protein trafficking	■ DNA repair	■ Nucleotide metabolism
■ Translation	■ Endoplasmic Reticulum	■ Mitochondria □ Lysosome
■ Lipid biosynthesis	■ Chromatin	■ Innate immunity ■ Other
■ Catabolic processes	■ Cell death	■ Reduction-oxidation

Figure 2.4: Functional categorization of ubiquitylated proteins.

(A) Functional categorization by biological process and cellular localization of all significant

proteins (≥two-fold change relative to mock infection, p<0.05) for *Mycobacterium*

tuberculosis infection.

(B) Functional categorization by biological process and cellular localization of all significant

proteins (≥two-fold change relative to mock infection, p<0.05) for *Listeria monocytogenes*

infection

(C) Functional categorization by biological process and cellular localization of all significant

proteins (≥two-fold change relative to mock infection, p<0.05) for *Salmonella typhimurium*

infection

Figure 2.5

a
L. monocytogenes
WT   Δ*hly*

b
S. typhimurium
WT   Δ*spi1/2*

c
M. tuberculosis
WT   Δ*esx1*

Scale (log$_2$)
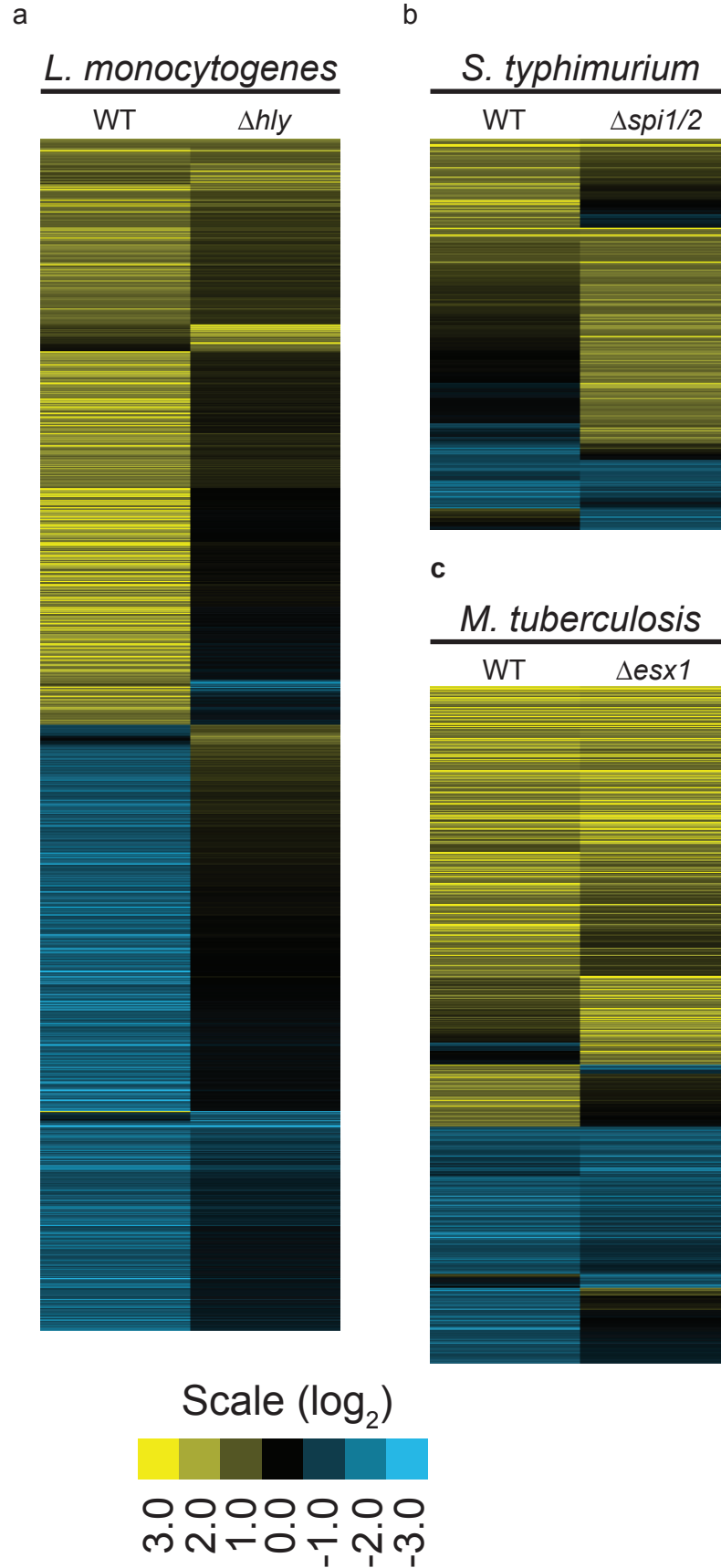
3.0 2.0 1.0 0.0 -1.0 -2.0 -3.0

Figure 2.5: Lysine-site ubiquitylation in response to bacterial virulence.

(A) Heat map of the average log2 fold change in ubiquitylation for each lysine site detected in wild-type (wt) and ΔHLY *Listeria monocytogenes* infections that was significant (≥two-fold change relative to mock infection, p<0.05) in at least one infection.

(B) Heat map of the average log2 fold change in ubiquitylation for each lysine site detected in wild-type (wt) and ΔssAVΔorgA (Δspi1/2) *Salmonella typhimurium* infections that was significant (≥two-fold change relative to mock infection, p<0.05) in at least one infection.

(C) Heat map of the average log2 fold change in ubiquitylation for each lysine site detected in wild-type (wt) and ΔEccD (Δesx1) *Mycobacterium tuberculosis* infections that was significant (≥two-fold change relative to mock infection, p<0.05) in at least one infection.
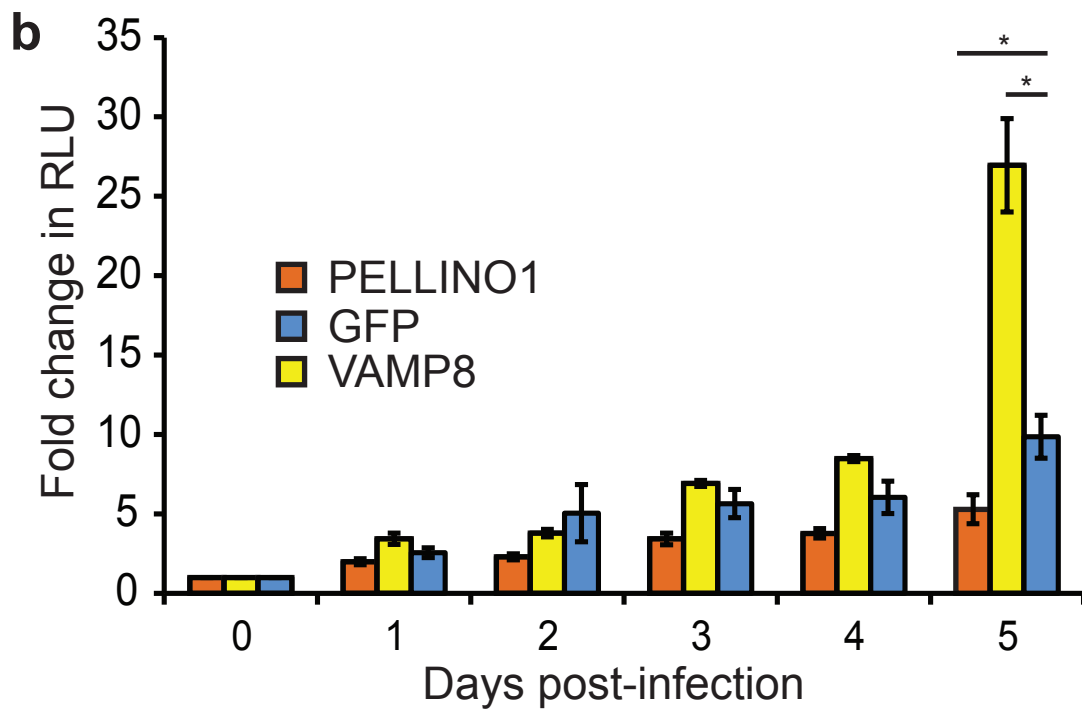
Figure 2.6

Figure 2.6: Ubiquitin targets that modify *Mycobacterium tuberculosis* replication in macrophages.

(A) J774 mouse macrophages stably overexpressing OASL1, GFP, or RENR were infected with autoluminescent *Mycobacterium tuberculosis* and luminescence was monitored every 24 hours and values plotted as fold change relative to t=0.

(B) J774 mouse macrophages stably overexpressing PELLINO1, GFP, or VAMP8 were infected with autoluminescent *Mycobacterium tuberculosis* and luminescence was monitored every 24 hours and values plotted as fold change relative to t=0. All measurements shown as means ± s.e.m. *p<0.05, **p<0.005, ***p<0.0005 by two-tailed Student's t-test.

Figure 2.7

a
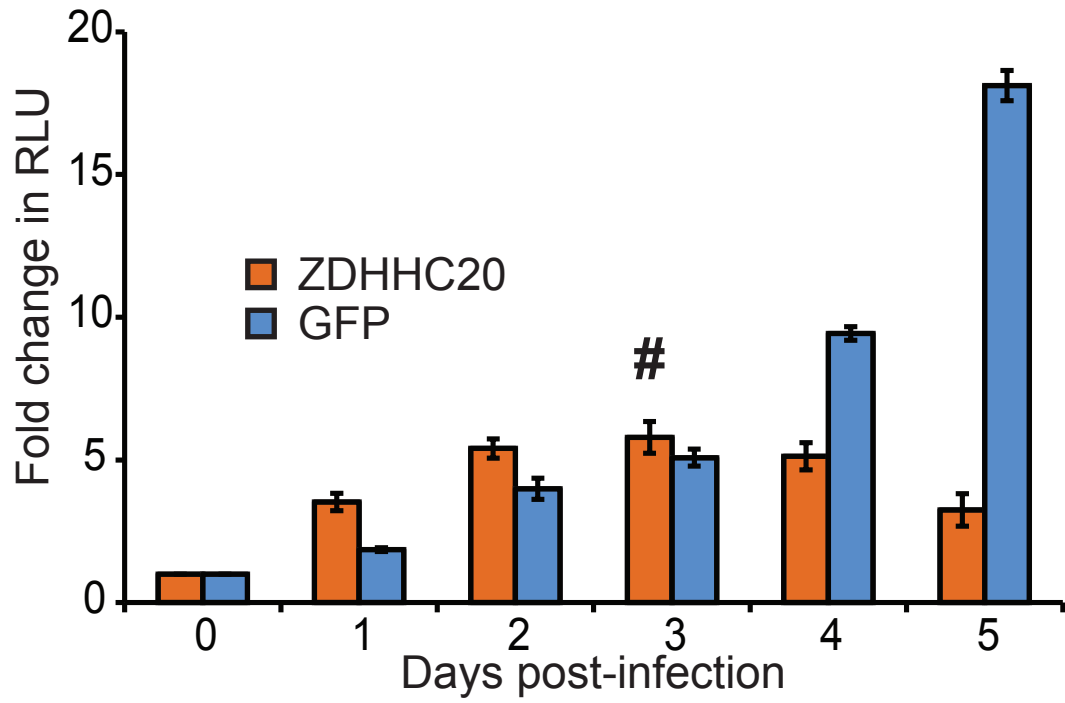
b
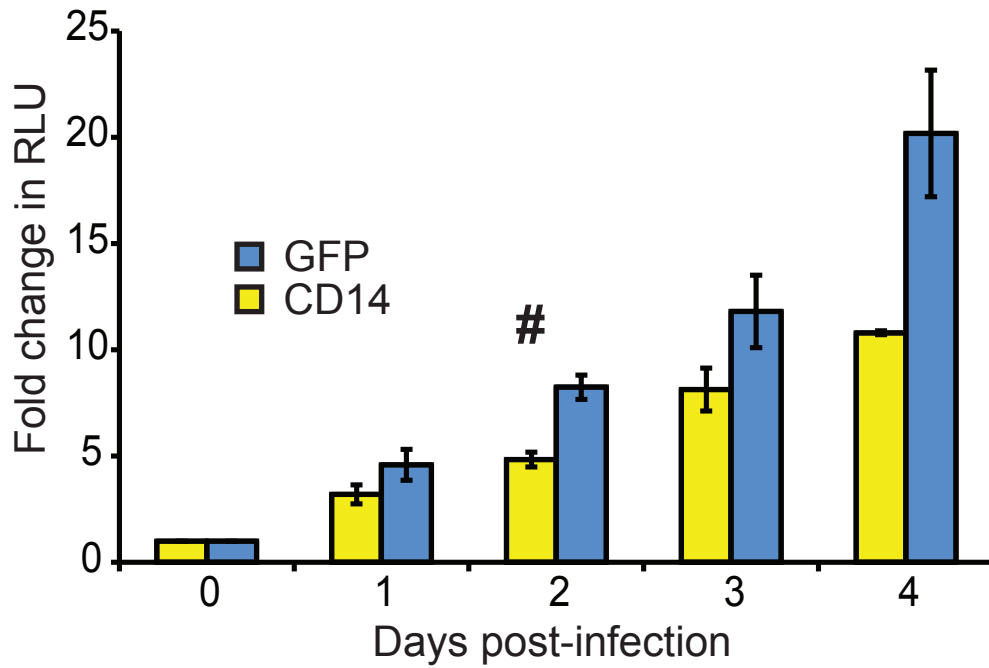
Figure 2.7: Ubiquitin targets that induce macrophage lysis after infection with

*Mycobacterium tuberculosis***.**

(A) J774 mouse macrophages stably overexpressing ZDHHC20 or GFP were infected with

autoluminescent *Mycobacterium tuberculosis* and luminescence was monitored every 24

hours and values plotted as fold change relative to t=0.

(B) J774 mouse macrophages stably overexpressing CD14 or GFP were infected with

autoluminescent *Mycobacterium tuberculosis* and luminescence was monitored every 24

hours and values plotted as fold change relative to t=0. All measurements shown as means $\pm$

s.e.m. #=at least 50% reduction in monolayer integrity relative to GFP-expressing cells.

Figure 2.8

a

Relative OASL1 levels:　　1　　0.55

b

c
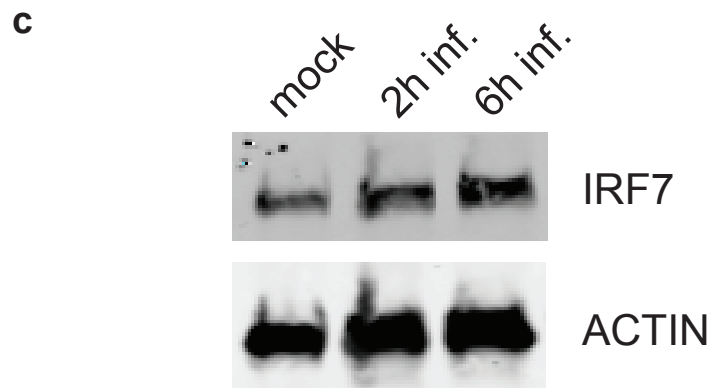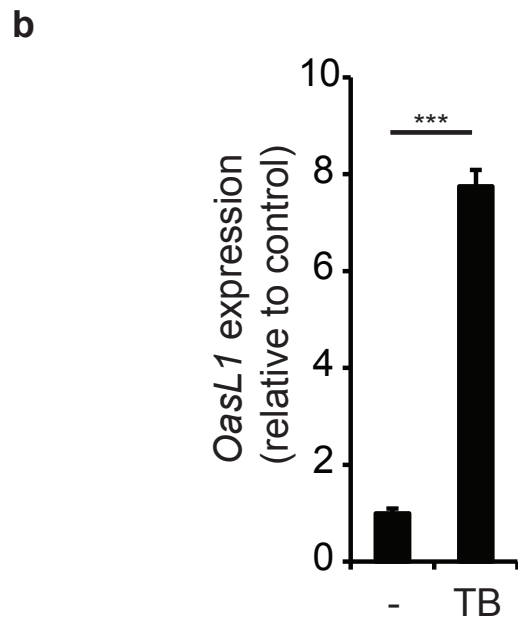
Relative IRF7 levels:　　1　　1.55　　1.57

Figure 2.8: OASL1 is inactivated at six hours post-infection.

(A) OASL1 and ACTIN protein levels were determined by western blot from mouse bone marrow-derived macrophages that were mock infected (-) or *Mycobacterium tuberculosis* infected (TB) for six hours.

(B) OasL1 mRNA levels were assessed by RT-qPCR amplification at six hours in mock infected (-) or *M. tuberculosis* infected (TB) bone marrow-derived macrophages and data are expressed as a fold increase in expression relative to mock infected (control) cells.

(C) IRF7 and ACTIN protein levels were determined by western blot from mouse bone marrow-derived macrophages that were mock infected or *Mycobacterium tuberculosis* infected for two or six hours. All measurements shown as means ± s.e.m. ***$p < 0.0005$ by two-tailed Student's t-test. Proteins quantified relative to the ACTIN loading control.
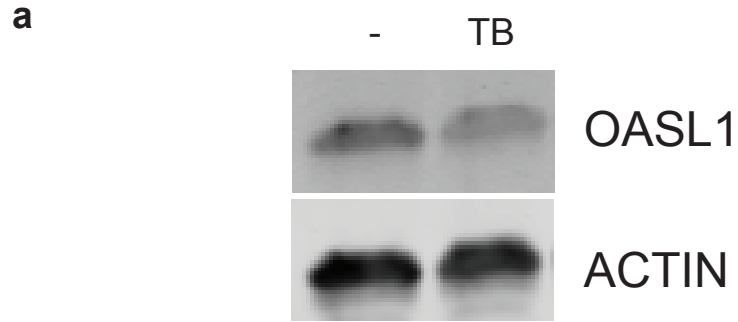
Figure 2.9

a
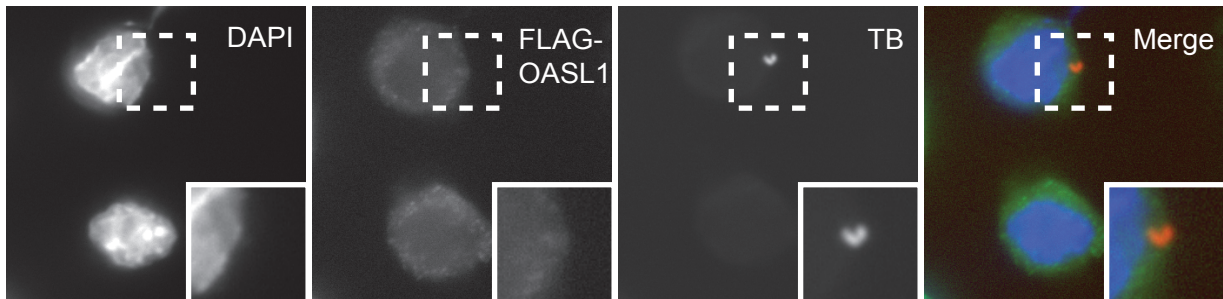
b
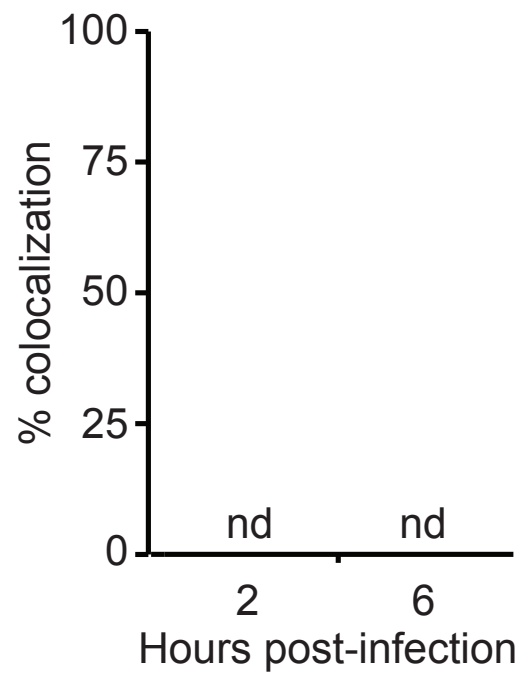
Figure 2.9: OASL1 does not localize to *Mycobacterium tuberculosis* during infection.

(A) Fluorescence images of FLAG$_3$-OASL1 overexpressing J774 macrophages, nuclei visualized with DAPI (blue), infected for six hours with mcherry-expressing *Mycobacterium tuberculosis* (red) and immunostained with an anti-FLAG antibody (green).

(B) Quantitative analysis of colocalization with OASL1 at two and six hours post-infection. nd=none detected.

Figure 2.10

a
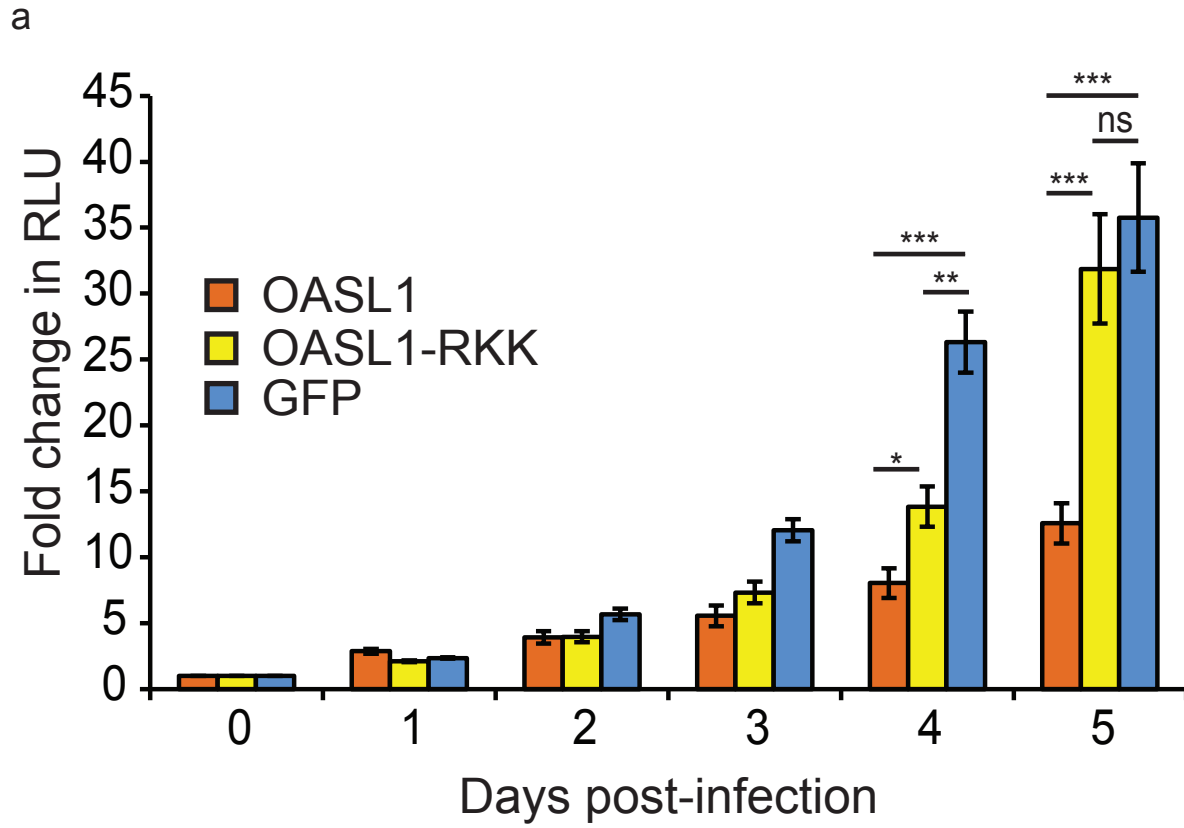
Figure 2.10: OASL1 requires its RNA-binding activity to suppress *Mycobacterium tuberculosis* growth.

(A) J774 mouse macrophages stably overexpressing GFP, OASL1, or an RNA-binding deficient OASL1 mutant (OASL1-RKK) were infected with autoluminescent *Mycobacterium tuberculosis* and luminescence was monitored every 24 hours and values plotted as fold change relative to t=0. All measurements shown as means ± s.e.m. ns=not significant, *p<0.05, **p<0.005, ***p<0.0005 by two-tailed Student's t-test.

Figure 2.11

a

Figure 2.11: OASL1 does not require a lysine residue at position 327to suppress

Mycobacterium tuberculosis **growth.**

(A) J774 mouse macrophages stably overexpressing GFP, OASL1, or a lysine to arginine OASL1 mutant at position 327 (OASL1-K327R) were infected with autoluminescent *Mycobacterium tuberculosis* and luminescence was monitored every 24 hours and values plotted as fold change relative to t=0. All measurements shown as means ± s.e.m. ns=not significant, *p<0.05, **p<0.005 by two-tailed Student's t-test.

Figure 2.12

a

b

Figure 2.12: *Irf7* shRNA knockdown suppresses *Mycobacterium tuberculosis* growth in J774 macrophages.

(A) J774 cells were transduced with lentiviral constructs expressing shRNAs targeting *Irf7* or scrambled shRNA (control) and stably selected. mRNA levels were assessed by RT-qPCR amplification and data are expressed as a percentage knockdown relative to control knockdown cells.

(B) J774 mouse macrophages stably overexpressing a scramble shRNA, or one of two shRNAs targeting *Irf7* mRNA were infected with autoluminescent *Mycobacterium tuberculosis* and luminescence was monitored every 24 hours and values plotted as fold change relative to t=0. All measurements shown as means ± s.e.m. ns=not significant, *p<0.05, **p<0.005, ***p<0.0005 by two-tailed Student's t-test.
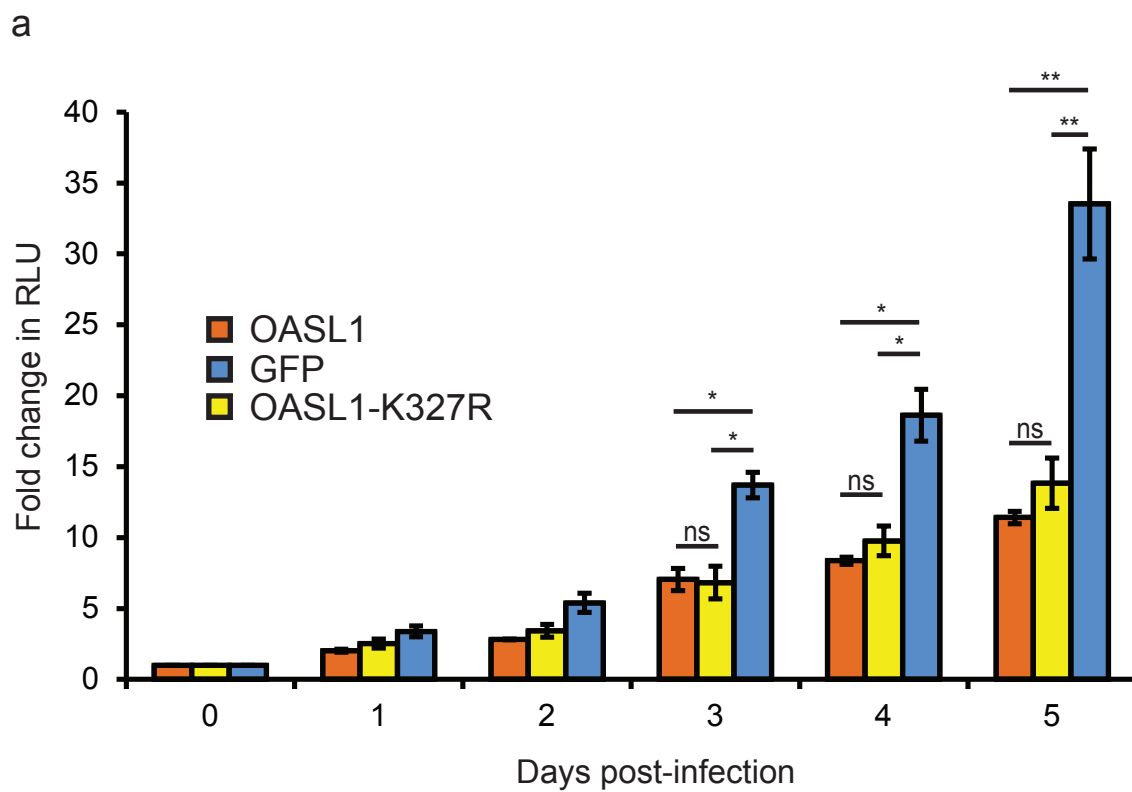
Figure 2.13

Figure 2.13: IRF7 expression rescues the *Mycobacterium tuberculosis* growth defect in cells overexpressing OASL1.

(A) J774 mouse macrophages stably overexpressing OASL1 and co-selected to overexpress GFP, IRF7 with its wild-type 5'UTR (wtUTR-IRF7), or IRF7 with an eight base pair mutation in its 5'UTR that disrupts the OASL1 binding site (mtUTR-IRF7) were infected with autoluminescent *Mycobacterium tuberculosis* and luminescence was monitored every 24 hours and values plotted as fold change relative to t=0.

(B) IRF7 and ACTIN protein levels were determined by western blot from RAW264.7 mouse macrophages stably expressing wtUTR-IRF7 or mtUTR-IRF7 in the presence and absence of exogenous OASL1. All measurements shown as means ± s.e.m. ns=not significant, **p<0.005, ***p<0.0005 by two-tailed Student's t-test. Proteins quantified relative to ACITN loading control.

Figure 2.14

a

b
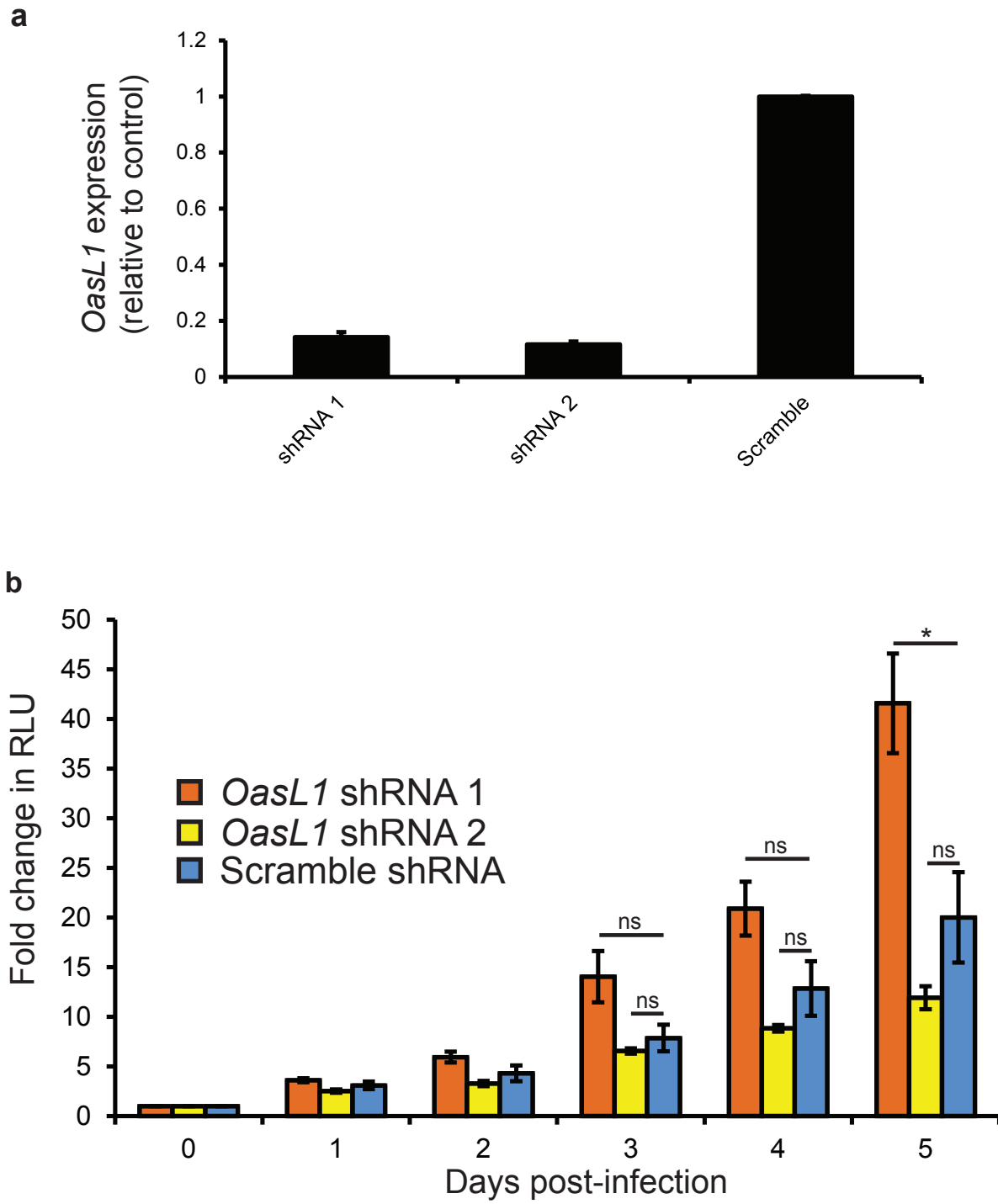
Figure 2.14: *OasL1* **shRNA knockdown has no consistent effect on** *Mycobacterium tuberculosis* **growth in J774 macrophages.**

(A) J774 cells were transduced with lentiviral constructs expressing shRNAs targeting *OasL1* or scrambled shRNA (control) and stably selected. mRNA levels were assessed by RT-qPCR amplification and data are expressed as a percentage knockdown relative to control knockdown cells.

(B) J774 mouse macrophages stably overexpressing a scramble shRNA, or one of two shRNAs targeting *OasL1* mRNA were infected with autoluminescent *Mycobacterium tuberculosis* and luminescence was monitored every 24 hours and values plotted as fold change relative to t=0. All measurements shown as means ± s.e.m. ns=not significant, *p<0.05, by two-tailed Student's t-test.
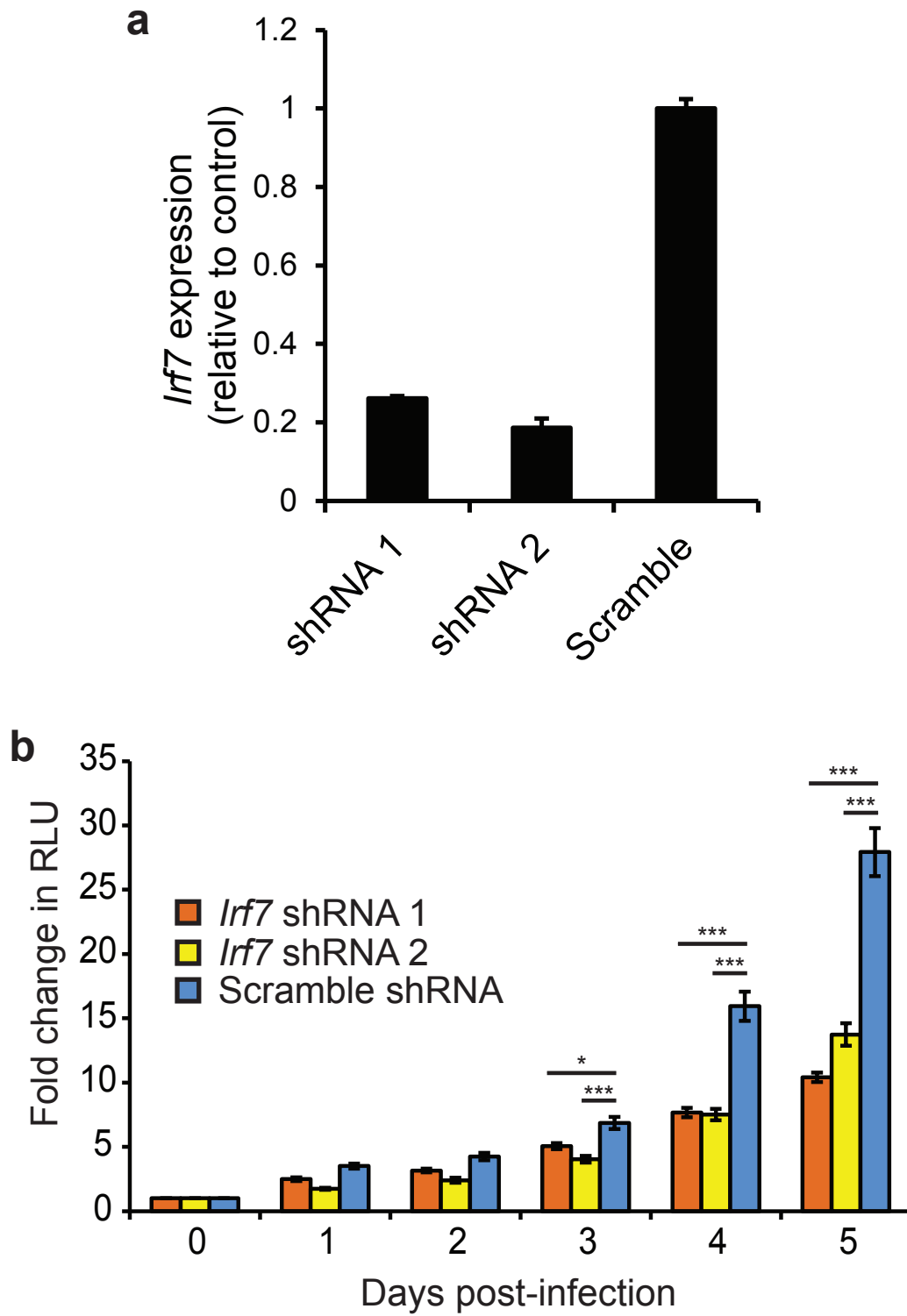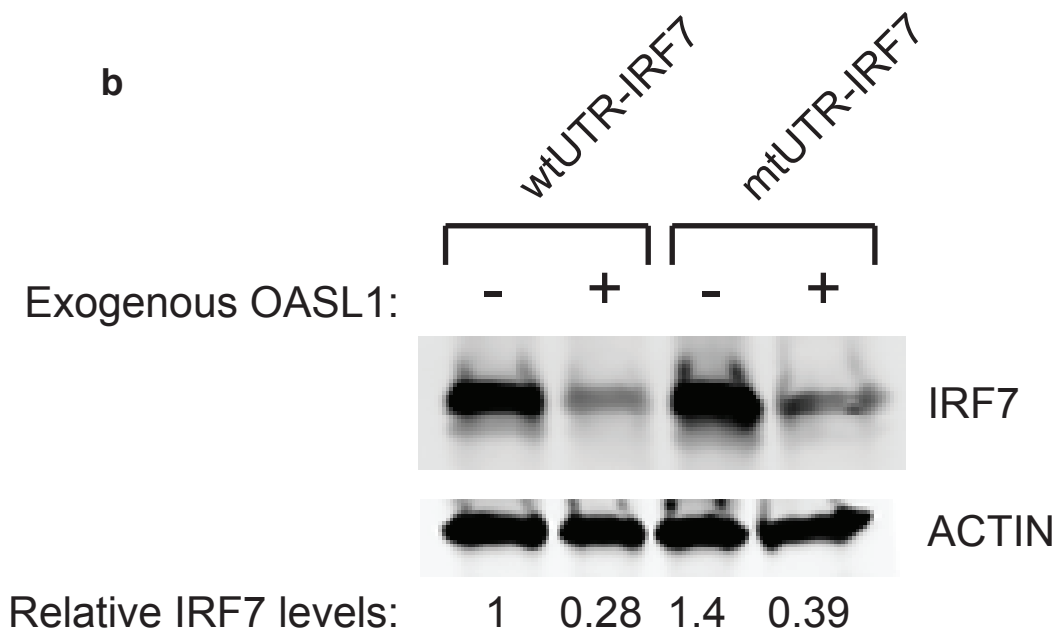
Figure 2.15

a
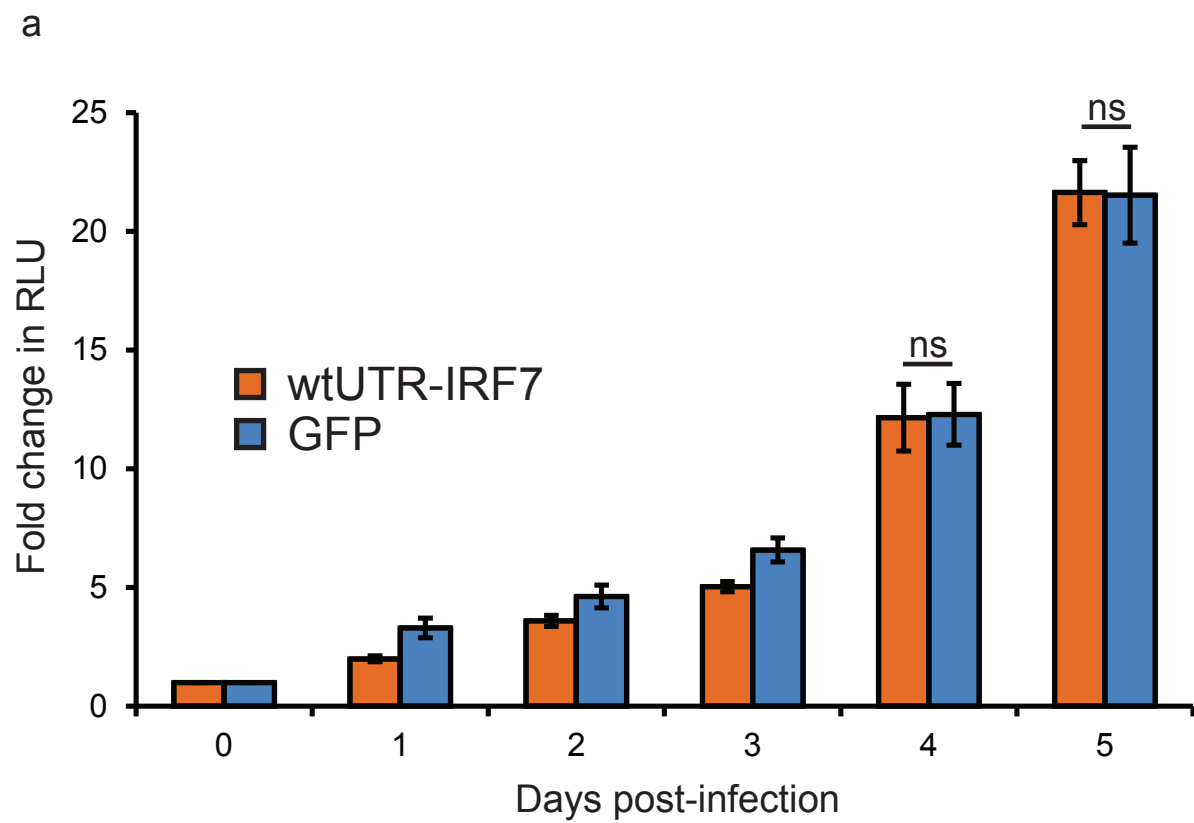
Figure 2.15: IRF7 overexpression has no effect on *Mycobacterium tuberculosis* growth in J774 macrophages.

(A) J774 mouse macrophages stably overexpressing wtUTR-IRF7 or GFP were infected with autoluminescent *Mycobacterium tuberculosis* and luminescence was monitored every 24 hours and values plotted as fold change relative to t=0. All measurements shown as means ± s.e.m. ns=not significant by two-tailed Student's t-test.
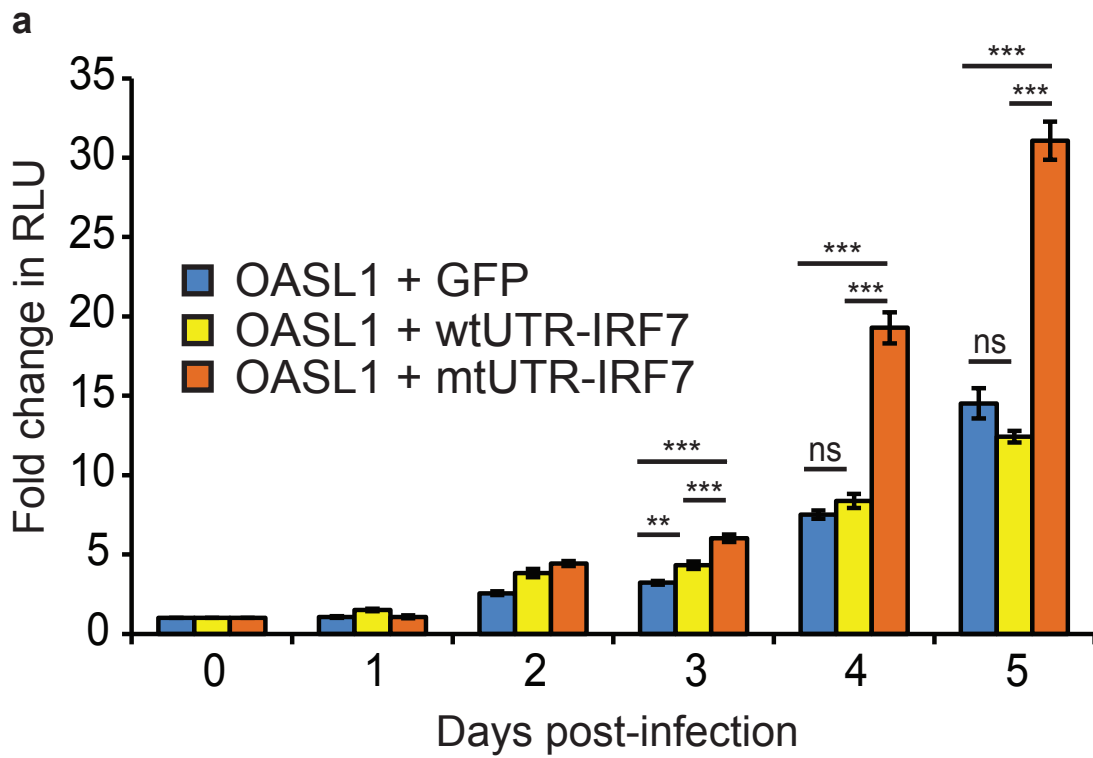
Figure 2.16

a
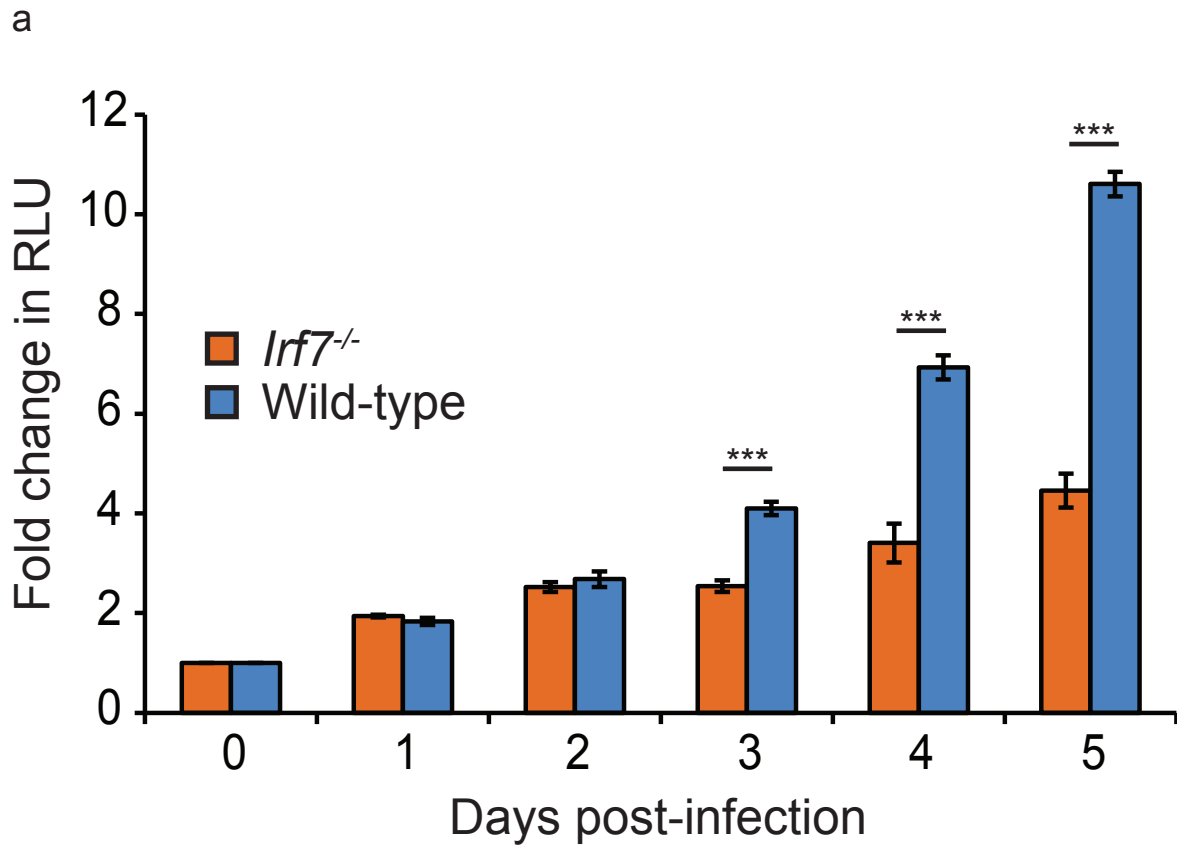
Figure 2.16: *Irf7^{-/-}* **knockout bone marrow-derived macrophages are repressive to**

Mycobacterium tuberculosis **growth.**

(A) Bone marrow-derived macrophages elicited from wild-type or *Irf7^{-/-}* C57BL/6 mice were

   infected with autoluminescent *Mycobacterium tuberculosis* and luminescence was monitored

   every 24 hours and values plotted as fold change relative to t=0. All measurements shown as

   means ± s.e.m. ***p<0.0005 by two-tailed Student's t-test.

Figure 2.17

a

b
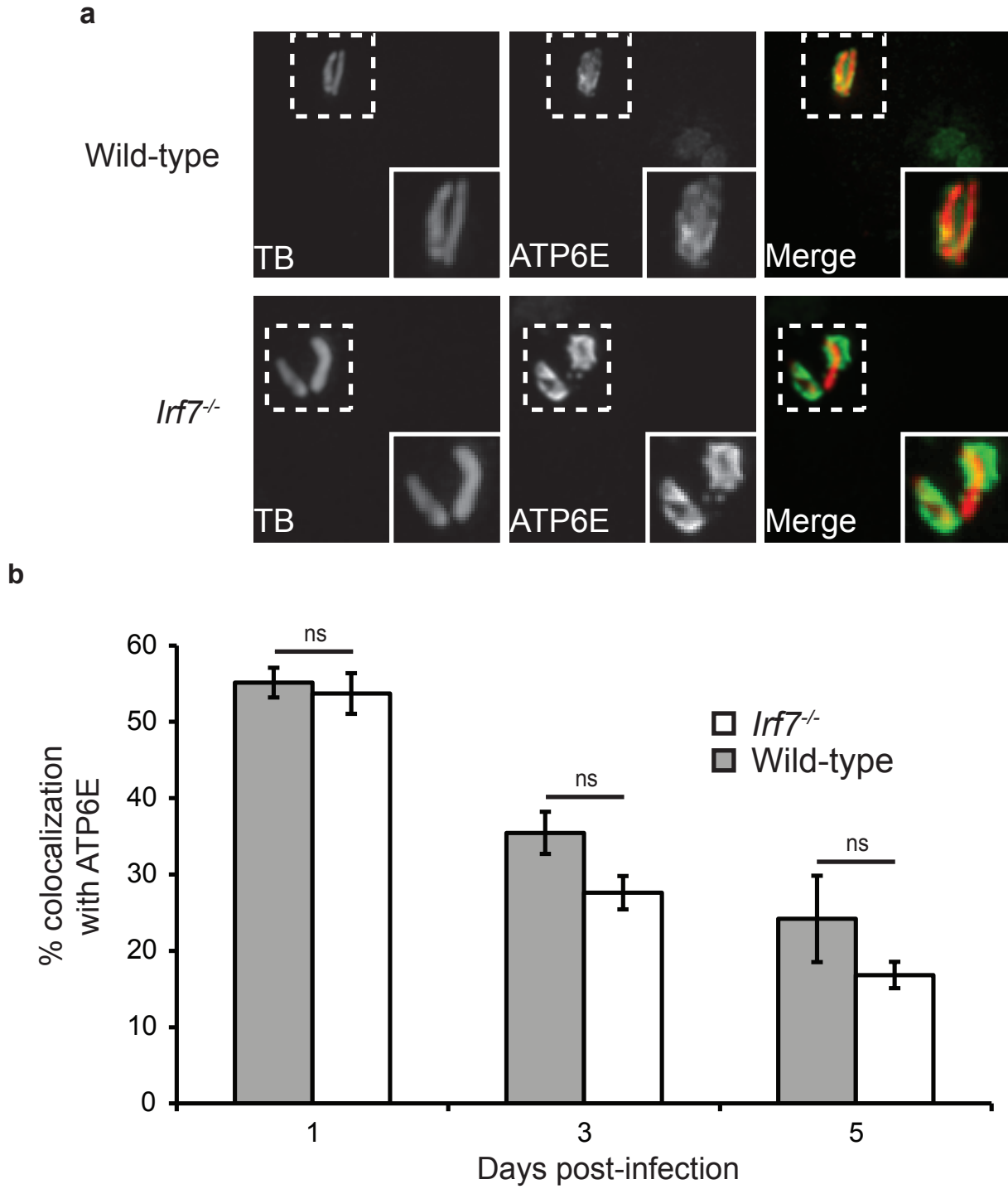
Figure 2.17: Lysosomal trafficking of *Mycobacterium tuberculosis* is unaltered in *Irf7*$^{-/-}$ knockout bone marrow-derived macrophages.

(A) Fluorescence images of wild-type or *Irf7*$^{-/-}$ knockout bone marrow-derived macrophages infected for 24 hours with mcherry-expressing *Mycobacterium tuberculosis* (red) and immunostained with anti-ATP6E antibody (green)

(B) Quantitative analysis of colocalization with ATP6E (the V-type ATPase) at 24, 72, and 120 hours post-infection. All measurements shown as means ± s.e.m. ns=not significant by two-tailed Student's t-test.

Figure 2.18

a
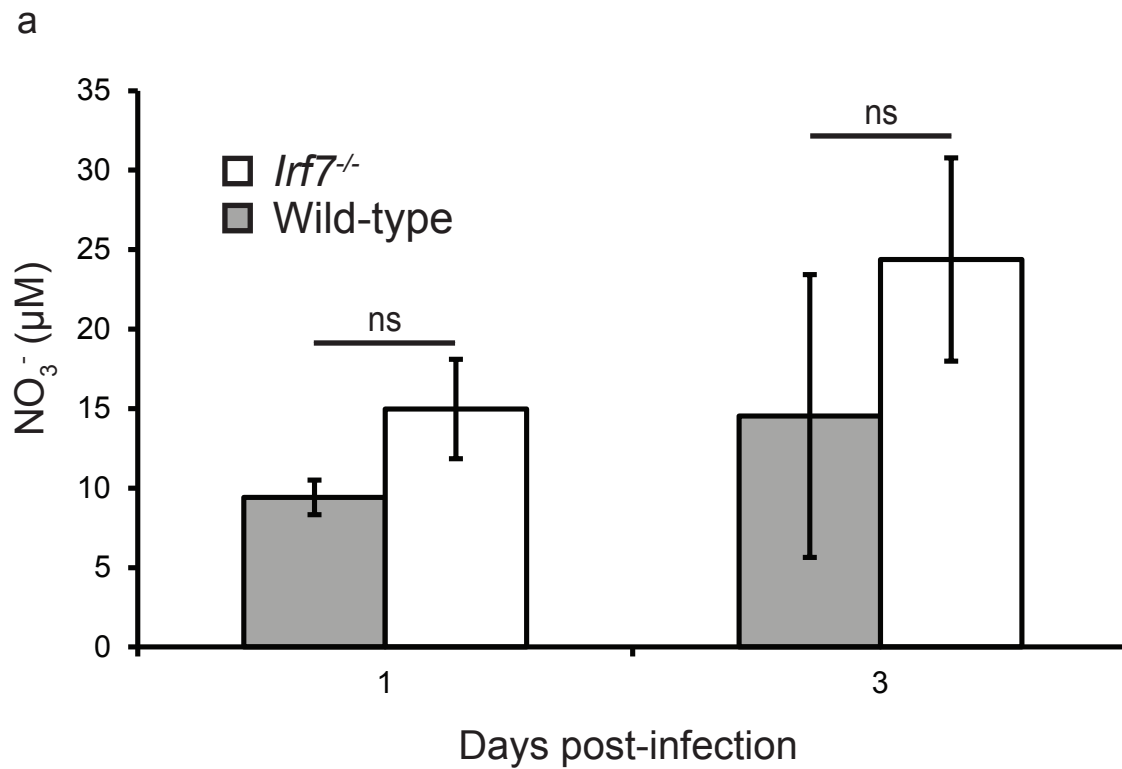
Figure 2.18: Nitric oxide production is unaltered in *Irf7*^{-/-} knockout bone marrow-derived macrophages.

(A) Quantitative analysis of nitric oxide production (as measured by Griess assay) at 24 and 72 hours post-infection in wild-type and *Irf7*$^{-/-}$ knockout bone marrow-derived macrophages. All measurements shown as means ± s.e.m. ns=not significant by two-tailed Student's t-test.

Figure 2.19
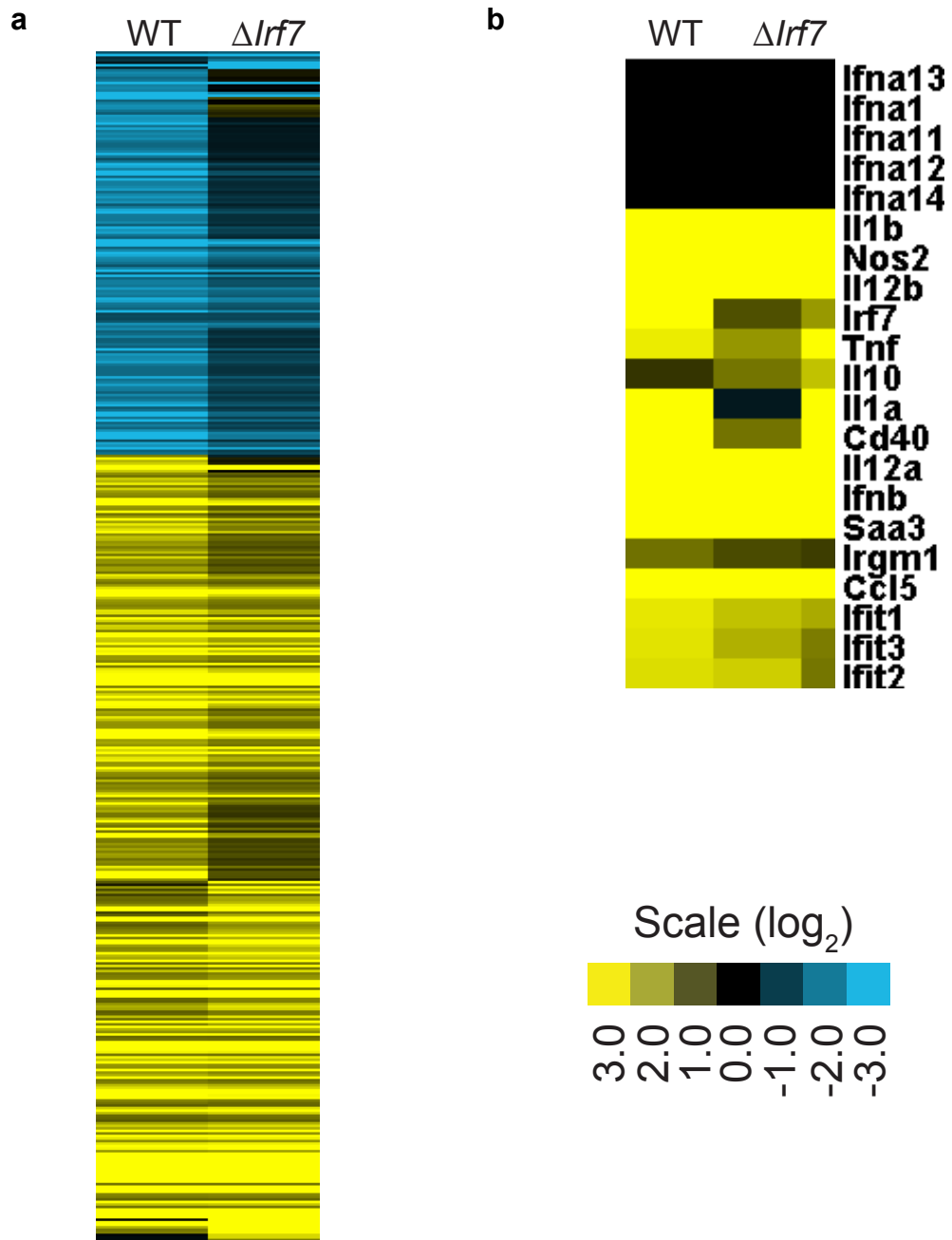
Figure 2.19: RNAseq analysis of wild-type and *Irf7$^{-/-}$* knockout bone marrow-derived macrophages infected for 24 hours.

(A) Heat map of all genes with at least a p<0.01 and a two-fold change (data analysis performed using Tophat suite of RNAseq tools) at 24 hours post-infection relative to mock infected control for wild-type and *Irf7$^{-/-}$* knockout bone marrow-derived macrophages.

(B) Heat map of a subset of genes from (a) that are critical for control of *Mycobacterium tuberculosis* infection or are known/predicted to be regulated by IRF7.

Figure 2.20
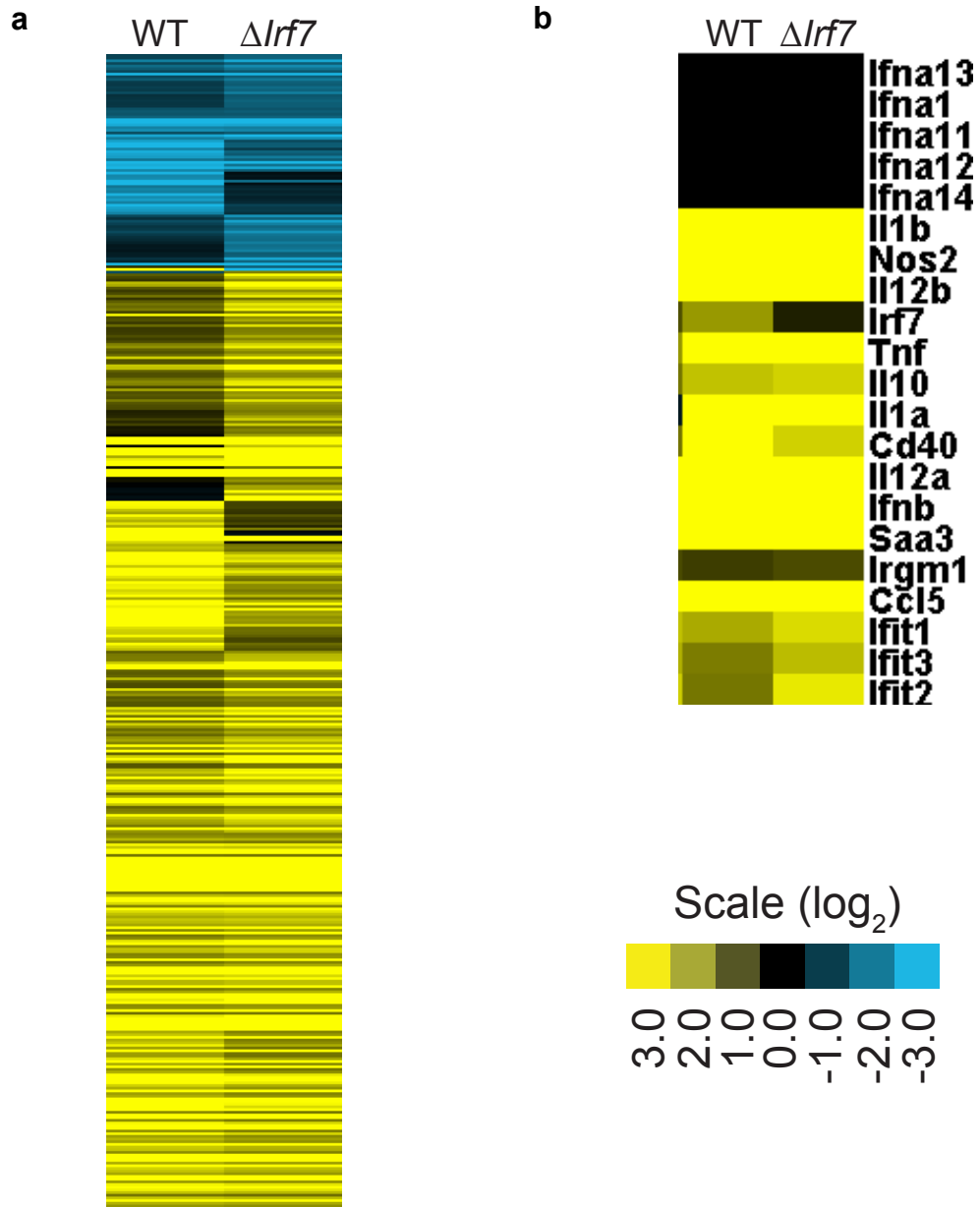
Figure 2.20: RNAseq analysis of wild-type and *Irf7^{-/-}* knockout bone marrow-derived macrophages infected for 72 hours.

(A) Heat map of all genes with at least a p<0.01 and a two-fold change (data analysis performed using Tophat suite of RNAseq tools) at 72 hours post-infection relative to mock infected control for wild-type and *Irf7^{-/-}* knockout bone marrow-derived macrophages.

(B) Heat map of a subset of genes from (a) that are critical for control of *Mycobacterium tuberculosis* infection or are known/predicted to be regulated by IRF7.

Figure 2.21

a
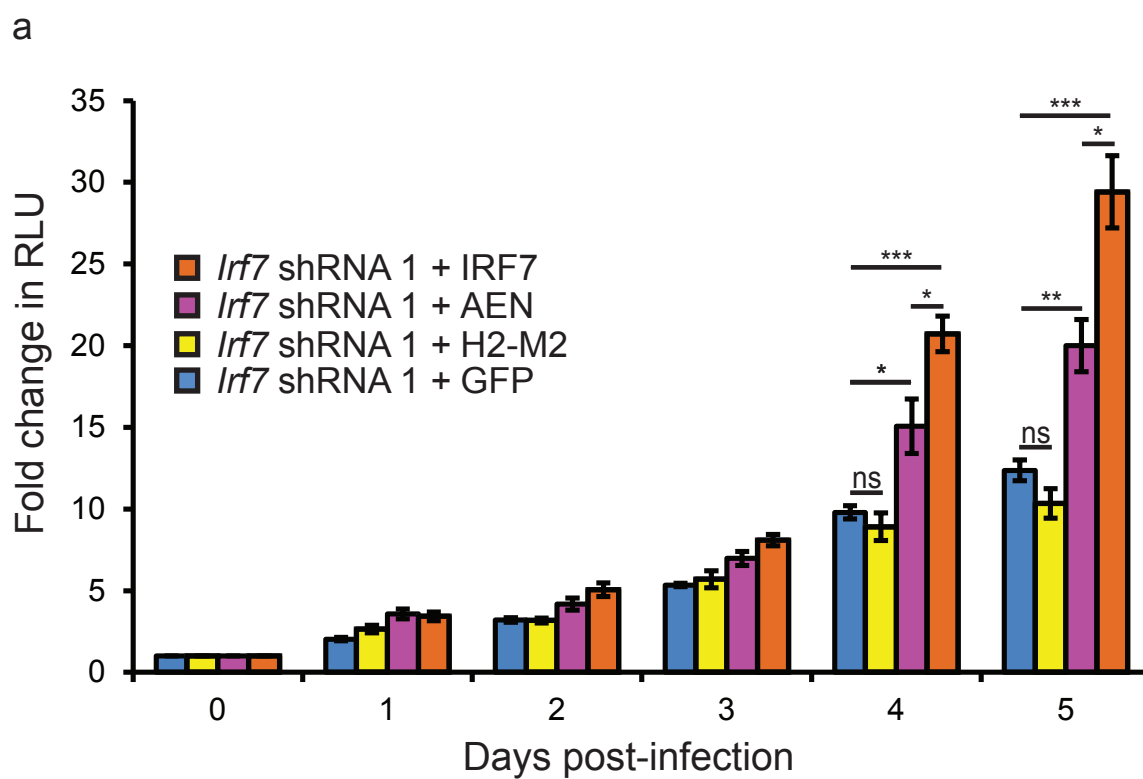
Figure 2.21: A functional screen of IRF7 transcriptional targets during *Mycobacterium tuberculosis* infection.

(A) J774 mouse macrophages stably overexpressing an shRNA targeting *Irf7* and co-selected to overexpress GFP, IRF7, AEN, or H2-M2 were infected with autoluminescent *Mycobacterium tuberculosis* and luminescence was monitored every 24 hours and values plotted as fold change relative to t=0. All measurements shown as means ± s.e.m. ns=not significant, *p<0.05, **p<0.005, ***p<0.0005 by two-tailed Student's t-test.

Figure 2.22

a

Flag$_3$-BirA-GFP

Flag$_3$-BirA-OASL1

Anti-Flag

Relative expresion: 7.6   1

b

Flag$_3$-OASL1

Flag$_3$-BirA-GFP

Flag$_3$-BirA-OASL1

Steptavidin-800
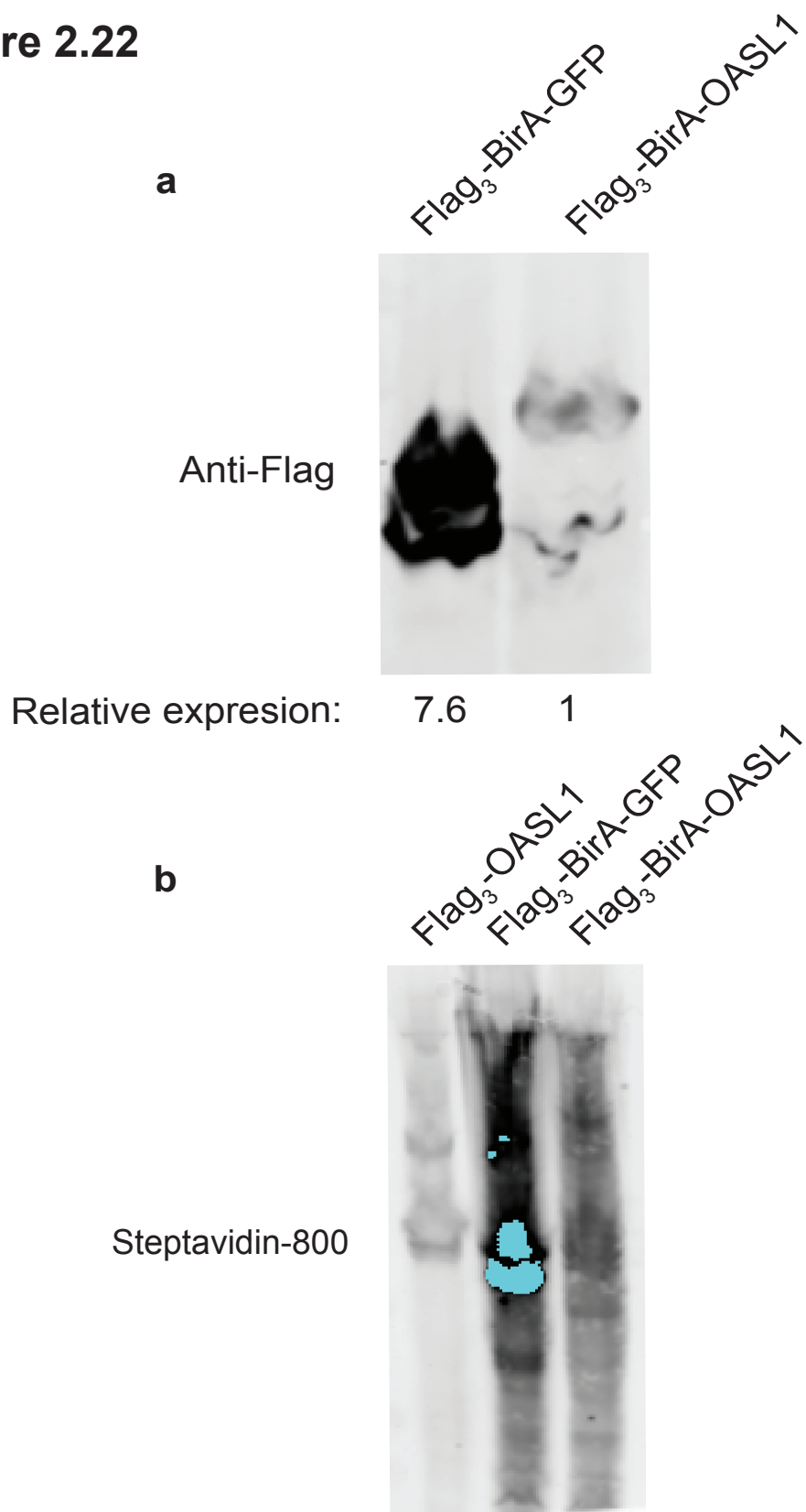
Figure 2.22: Identifying IRF7 interactors by using a promiscuous BirA fusion protein.

(A) Protein levels of lysates from RAW264.7 mouse macrophages stably overexpressing FLAG3-BirA-GFP or FLAG3-BirA-OASL1 fusion proteins were determined by western blot using an anti-FLAG antibody. Proteins quantified relative to FLAG3-BirA-OASL1.

(B) Detection of biotinylated substrates in RAW264.7 mouse macrophages overexpressing FLAG3-OASL1, FLAG3-BirA-GFP, or FLAG3-BirA-OASL1 and treated for 24 hours with biotin were determined by western blot using infrared dye-labelled streptavidin (streptavidin-800).

Figure 2.23
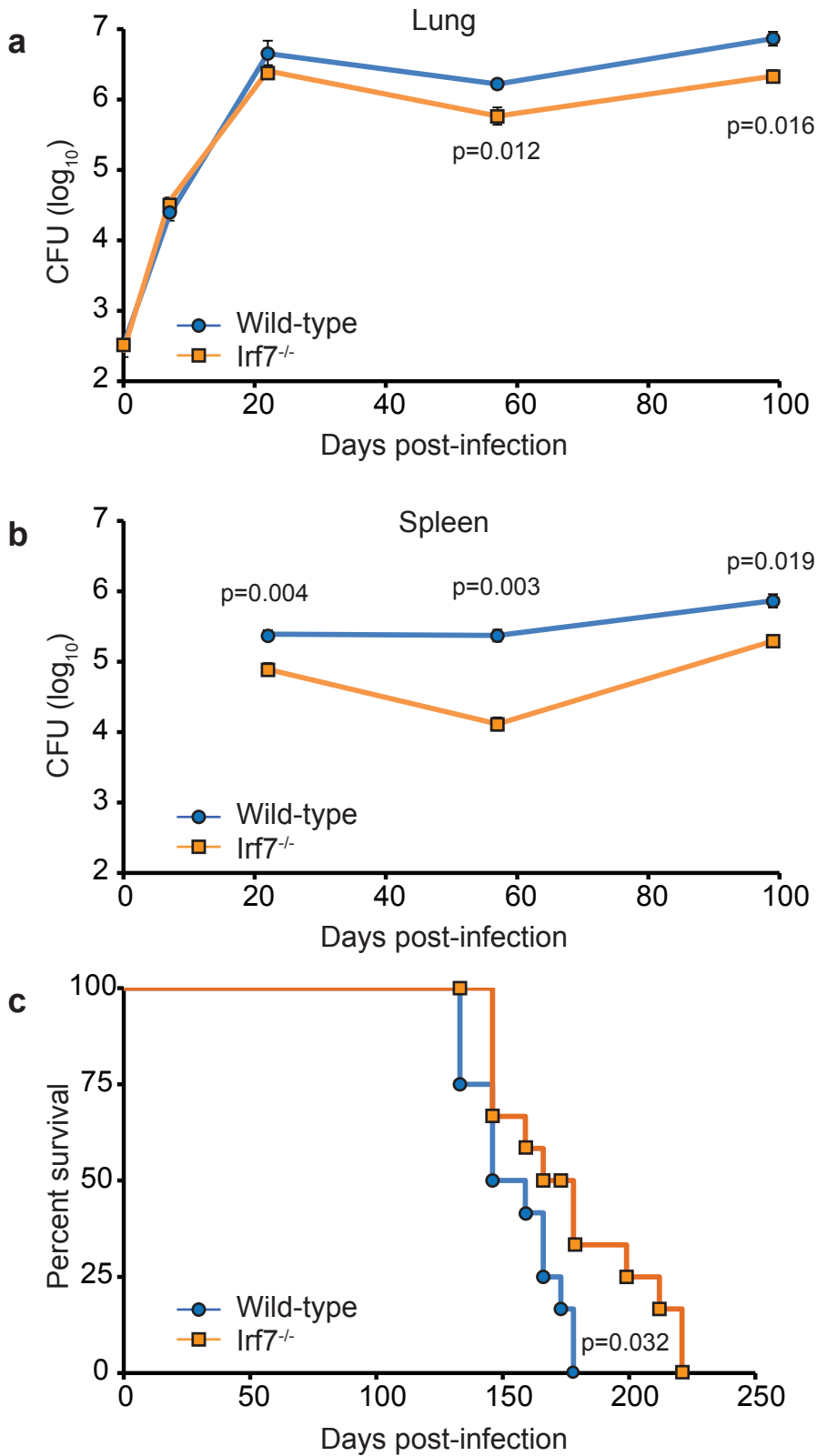
Figure 2.23: *Irf7*$^{-/-}$ **knockout mice are resistant to** *Mycobacterium tuberculosis* **infection** *in vivo.*

(A) Wild-type and *Irf7*$^{-/-}$ knockout mice were infected with *Mycobacterium tuberculosis* via the aerosol route, and lung bacterial burdens were determined by plating at days 0, 7, 22, 57 and 99 (means ± s.e.m. n=4 per group, p values calculated by two-tailed Student's t-test).

(B) Enumeration of spleen c.f.u. from mice infected in (a)**,** at days 22, 57, and 99 (means ± s.e.m. n=4 per group, p values calculated by two-tailed Student's t-test).

(C) Survival analysis of infected wild-type and *Irf7*$^{-/-}$ knockout mice (n=12 per group, p values calculated by log-rank test).

Figure 2.24

a
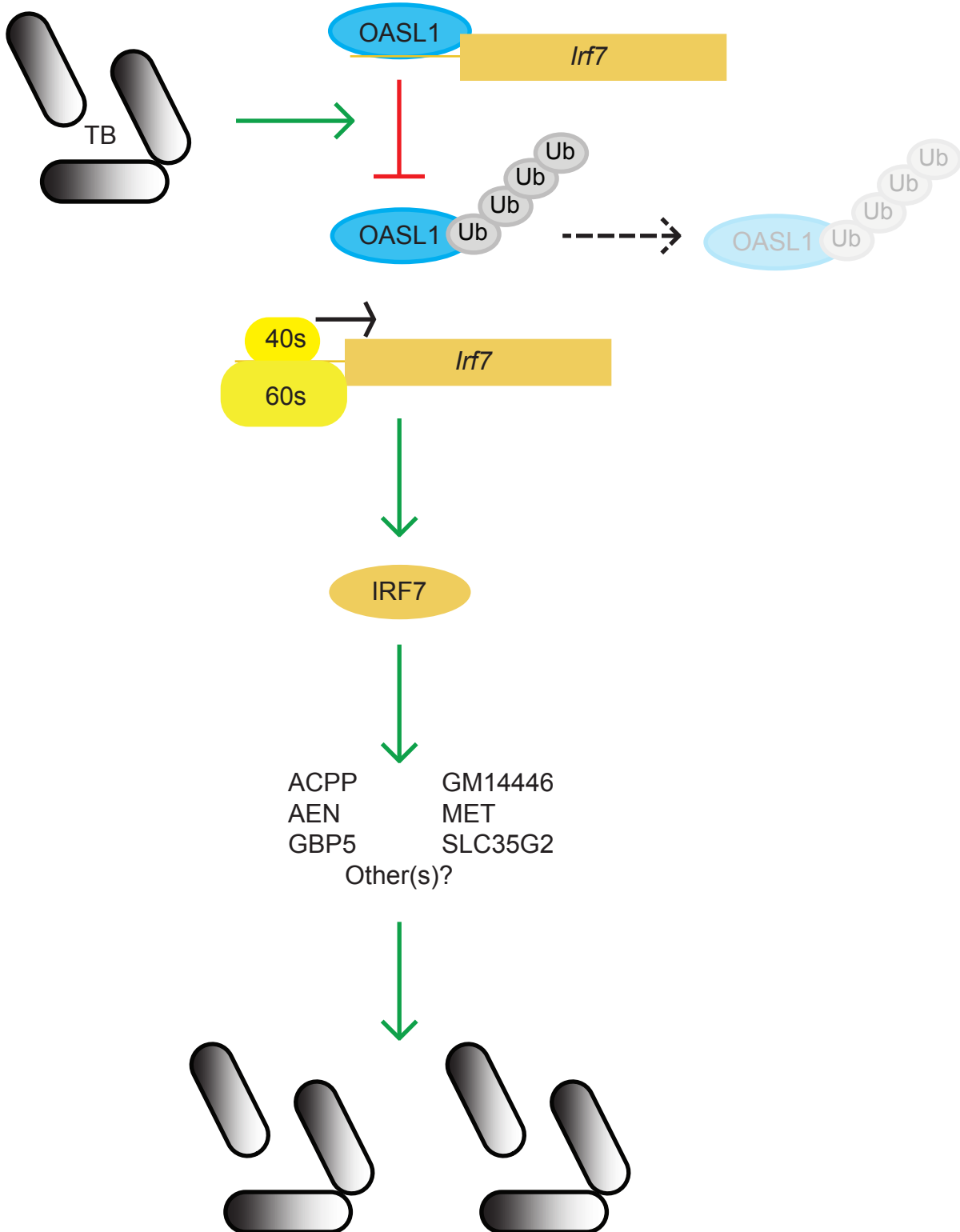
Figure 2.24: A model for the regulation of OASL1 and IRF7 in *Mycobacterium tuberculosis* infected macrophages.

(A) Upon phagocytosis of *Mycobacterium tuberculosis* by macrophages, OASL1 is ubiquitylated and degraded by the proteasome. This allows access of the ribosome to all of the mRNAs previously bound by OASL1, including Irf7. Translation of IRF7 allows this transcription factor to translocate to the nuclease and activate at least 57 transcripts, while repressing at least 12 others. Six (or more) of the genes targeted by IRF7 participate in allowing *Mycobacterium tuberculosis* to replicate in macrophages: ACPP, AEN, GBP5, GM14446, MET, and SLC35G2.

Chapter 3: Ongoing projects

Global phosphorylation of the macrophage proteome during intracellular bacterial pathogen infection

Phosphorylation acts as an important signal during all stages of life in a cell, including during infection with bacterial pathogens (Ribet and Cossart 2010). Additionally, bacteria are known to extensively modify host phosphorylation to help promote and establish infection (Krachler et al. 2011). Understanding changes in global phosphorylation to the host cell during infection has been of interest to the field for a long time, and advances in mass spectrometry has provided a platform to begin to dissect global phosphoproteomics during bacterial infection (Schmutz et al 2013, Yang et al. 2015). Indeed, global phosphoproteomics has been performed on macrophages infected with wild-type and secretion deficient *Salmonella,* identifying a number of pathways that are likely modified by SpiII effector proteins (Rodgers et al. 2011, Imami et al. 2013).

Fortunately for us, the method used to prepare samples for global ubiquitin profiling is identical to global phospho-peptide profiling. We prepared excess protein lysate when preparing our UbiScan experiments, and processed them to identify global changes in macrophage phosphorylation during infection with wild-type *M. tuberculosis, L. monocytogenes,* and *S. typhimurium* (figure 3.1). We are still waiting for a similar statistical analysis to be performed on our global phosphorylation data, so we have defined a "real" change in phosphorylation to any site that has a greater than two-fold change relative to mock infection. We were interested to see

if the phosphorylation patterns observed during infection with our three pathogens would look as distinct as the ubiquitylation pattern for these pathogens. Interestingly, the pattern of global phosphorylation looks more similar than the ubiquitylation pattern, but there is still a remarkable amount of specificity to each infection (figure 3.2). The similarities may arise from common kinase signaling cascades (like MAP and PI3 kinase signaling) and NFκB signaling initiated through engagement of the TLRs. In parallel to processing phosphoproteomic samples of wild-type infections, we used the same defined bacterial mutants to identify phosphorylation that required cytoplasmic access and effector delivery (figure 3.3). Much like the ubiquitylation analysis, *L. monocytogenes* infection induced the most robust phosphorylation signaling (in terms of total detected peptides relative to other infections), but the differences were not nearly as pronounced as with ubiquitin signaling. Additionally, the ΔHLY mutant induced much more phosphorylation signaling than is does ubiquitin signaling. While the wild-type and Δ*eccd* mutant *M. tuberculosis* infections looked the most similar when looking at ubiquitylation, they are the most distinct when looking at phosphorylation. A huge majority of phosphorylation observed during *M. tuberculosis* infection requires the ESX-1 secretion system. Wild-type and mutant *S. typhimurium* infections look almost indistinguishable (likely due to massive induction of TLR4 signaling because of the high levels of LPS present in these infections). We await a detailed statistical analysis before looking at functional categorization of hits like we did with the ubiquitin data.

While this global phosphoproteomics is fun to speculate about, we need to use this information to identify phosphorylation targets that are functionally relevant to infection. Like the ubiquitin screen, we chose a small number of proteins whose phosphorylation is changed dramatically during *M. tuberculosis* infection and stably overexpressed them in J774

macrophages. We tracked bacterial replication using our luciferase assay described in chapter two. Using this approach, we have identified two proteins that allow more robust bacterial replication when overexpressed in macrophages: IEX1 and BNIP3L (figure 3.4). We then chose IEX1 as a candidate to perform mutational analysis as a proof of concept for the larger screen that will be performed. IEX1 is phosphorylated at two sites, serine 18 and 31, in mock infected cells, and we observe a 582 and a 439 fold increase in phosphorylation on these serine residues after infection, respectively. We first made phosphomemetic serine to aspartic acid mutations to each serine individually and in combination, and infected these cells, comparing bacterial growth back to wild-type IEX1 overexpression (figure 3.5a). Interestingly, the S31D and double mutant expressing cells allowed more bacterial growth than wild-type IEX1, while overexpression of the S18D mutant made no difference. We also tested serine to alanine mutants at these sites alone and in combination to test the requirement of phosphorylation on our observed phenotype (figure 3.5b). Here we see that mutation of serine 18 to alanine allows more growth than wild-type IEX1, but the S31A and double mutant have no effect. This suggests that host phosphorylation of IEX1 in response to bacterial infection (particularly phosphorylated IEX1 at serine 31) is somehow beneficial to the bacteria. It will be important to determine what the biochemical function of IEX1 is, and to test the activity of the alanine and aspartic acid mutants to better understand the growth phenotype we are observing. This is only a representative set of experiments, and once we get better statistics done, we can pick new targets of phosphorylation/dephosphorylation to work on during infection. It will also be interesting to identify the signaling pathways that are shared and distinct for each bacterial species, and which of these pathways require the presence of a functional secretion system.

Ubiquitylation of bacterial proteins during infection

Early in my thesis project, I was interested in identifying the ubiquitylated protein(s) that appear around intracellular bacterial pathogens during infection. Much of my time was spent working out the conditions to perform the UbiScan experiments with multiple infections, but one of the earliest experiments I tried was to determine whether some or all of the ubiquitin was actually covalently attached to the bacteria themselves. As I was not yet trained to work in the BSL3, much of the work looking at potentially ubiquitylated bacterial substrates was done using *Mycobacterium marinum*, which is also ubiquitylated during infection of macrophages but is a BSL2 organism. The first question I asked was whether ubiquitin is maintained on bacteria isolated from macrophages at the peak of ubiquitylation after the host cells were lysed. To this end, I infected RAW 264.7 macrophages with wild-type *M. marinum* for six hours (the peak of ubiquitylation observed around these bacteria in this cell type). I harvested the macrophages and gently lysed them using TRIS/NaCl/1% NP40. I then cleared the supernatant of cellular debris by low speed centrifugation, then did a high speed spin to pellet the bacteria, and then resuspended the bacteria and spun them on to poly-lysine treated cover slips. These cover slips were then stained for ubiquitin (figure 3.6a). While approximately 30% of *M. marinum* are ubiquitylated in macrophages at six hours post-infection, I observed about 10% of the bacteria were ubiquitin positive after isolating them from infected cells (figure 3.6b). It was possible that we were falsely detecting ubiquitin positive bacteria due to random contamination of ubiquitin in our bacterial isolation preps, so I also isolated ΔRD1 *M. marinum* from infected cells as a negative control. The ΔRD1 strain lacks a functional ESX-1 secretion system, and is not ubiquitylated nearly as much as wild-type bacteria during infection (the number of ubiquitylated *M. marinum* at six hours in RAW264.7 cells is less than 5%). There were very few ubiquitylated

ΔRD1 bacteria, suggesting that the observed ubiquitin we were detecting on bacteria during wild-type infection was not due to contamination from free ubiquitin after cell lysis.

The next question was how the ubiquitin we see around the *M. marinum* after being isolated from macrophages is associated with the bacteria. It was possible the ubiquitylated host proteins that associate with/bind to the bacteria during infection were surviving bacterial isolation, so I wanted to try to remove the ubiquitin from the bacteria using a number of denaturing conditions. Fortunately, the physical structure of *Mycobacterial* species makes them highly resistant to lysis with denaturing agents, giving me a broad number to test to see if the observed ubiquitin could be removed from the bugs. At the time, I was using 8M urea to denature samples for another set of experiments, and tried to use this chemical treatment to remove the ubiquitin from the bacteria. After isolating the bacteria form macrophages as described above, I washed the bacterial pellets three times either with PBS or 8M urea in PBS, and then fixed them on cover slips and stained with an anti-ubiquitin antibody (figure 3.7a). While urea treatment did remove approximately 20% of the ubiquitin relative to PBS treatment, a majority of the ubiquitin remained associated with the bacteria (figure 3.7b). This suggested to us that at least some of the ubiquitin may be covalently attached to the bacteria themselves, and not bound to a host protein associated with the bacteria during infection as we had previously assumed. Since we already knew that the ubiquitin observed around the bacteria during infection was a mixture of both K48 and K63 linkages, we next wanted to test whether the covalently bound ubiquitin was enriched for one of these linkages, or if it was a mixture of both. I repeated the experiments as described above, but instead of immunostaining with antibodies that recognize all ubiquitin linkages (mono/poly), I tried using linkage specific antibodies to stain the bacteria. There was no observed difference in K48-linked ubiquitin colocalization with the

bacteria in the PBS vs. urea treatments, but what little K63-linked ubiquitin we saw around the bacteria when washed with PBS was completely removed when washed with urea (figure 3.7a and b). I also tried using high concentrations of Triton X100 and SDS to denature and remove the ubiquitin and got similar results.

Because the K48-linked ubiquitin stayed associated with the bacteria through harsh chemical treatment, I next sought out to determine if we could see ubiquitylated proteins from these treated bacteria by western blot. I isolated *M. marinum* from infected macrophages and washed thoroughly with 8M urea/PBS, and then lysed the bugs and identified ubiquitin-positive proteins by western blot. Lysates from wild-type bacteria isolated from infected cells revealed a number of ubiquitylated bands, and importantly, lysates from ESX-1 mutant bacteria had significantly reduced ubiquitylation (figure 3.8a). I also stained the western blots for the bacterial protein GroEL to ensure that the lanes were evenly loaded and that we were indeed looking at bacterial lysates. At this time, I had begun doing infection with *M. tuberculosis* in the BSL3, and wanted to know if we could observe ubiquitylated *M. tuberculosis* like we could with *M. marinum*. Using the same technique described above, I isolated and lysed wild-type and ESX-1 mutant *M. tuberculosis* from infected RAW264.7 macrophages, and saw the same enrichment for ubiquitylated proteins by western blot in the wild-type lysates (figure 3.8b).

I scaled these experiments up significantly, infection 24 15 cm^2 dishes of macrophages with a total of 3 billion bacteria, isolated the bugs, denatured using urea, and then lysed the bacteria and performed di-gly ubiquitin remnant immunoaffinity capture of any previously ubiquitylated bacterial proteins (same protocol as used in the UbiScan experiments). The Krogan lab performed mass spectrometry on these samples, and we identified six bacterial proteins that had previously ubiquitylated lysine residues: lysine 168 of Rv0180c, lysine 60 of Rv1307, lysine

456 of Rv2196, lysine 504 of Rv0206c, lysine 28 of Rv3264c, and lysine 428 of Rv3270. It was satisfying to see that all six proteins are surface exposed proteins (five membrane proteins and one periplasmic protein). When we mapped the predicted topology of these proteins, all of the lysine residues would be extracellular, confirming that the host would have access to these proteins in unlysed bacteria. The concern is that if these bacteria were healthy, the mycolic acid layer would separate these proteins from the host cytoplasm, and it is difficult to imagine how the host gains access to these lysine sites. It is possible that the host has one or more E3 ligases that can translocate across the mycolic acid layer and interact with proteins in the periplasm. It is also possible that the loops on which the ubiquitylated lysine residues reside somehow stick past the mycolic acids and are in direct contact with the cytoplasm. I think it is most likely that the bacteria that are getting ubiquitylated with K48 linked ubiquitin are somehow damaged (maybe these bacteria are sick or dead when infecting the cell, or are damaged by antimicrobial agents in the host). I believe the ubiquitylation observed here is not a specific interaction of the host with a bacterial protein, but recognition of a protein that should not be present in the host and the host is trying to destroy it through the proteasome. It would be interesting to look at the E3 ligases that have been implicated in residing inside the *M. tuberculosis* containing phagosome (Trost et al. 2009) and determine if the bacteria can be ubiquitylated in the absence of these ligases in cells, or if the ligases can ubiquitylate these proteins when purified.

One other potential site of ubiquitylation on the bacteria is on a subset of bacterial surface lipids. Some bacteria, including bacterial pathogens like *M. tuberculosis* and *L. monocytogenes*, harbor a special subset of lipids on their surfaces that have terminal lysine residues attached to them (Maloney et al. 2009, Thedieck et al. 2006). When these bacteria infect their host, the lysine residues of these lipids would be exposed to the cytoplasm of the host cell, and provide a

potential site for covalent attachment of ubiquitin as an anti-bacterial defense mechanism. To test

this, I obtained a transposon mutant of Rv1640c, the gene coding for the enzyme lysinylates

these lipids, in the H37rv *M. tuberculosis* strain. I infected bone marrow-derived macrophages

for six hours with wild-type and mutant H37rv, and stained these cells for ubiquitin (figure 3.9a),

looking for a defect in ubiquitin localization to the mutant. While there was a decrease in

ubiquitin colocalization with the mutant bacteria relative to wild-type, the difference was small

and not statistically different (figure 3.9b). I did not check for proper transposon insertion in this

strain so it is possible that the mutant we received from the Stanley lab is not in Rv1640c. It may

also be worth testing the other two clones I picked of the mcherry positive 1640c strain (as well

as the wild-type strain made in parallel), but as it stands, I believe that the bacterial proteins

identified by mass spectrometry are likely the only sites of ubiquitylation covalently attached to

M. tuberculosis in macrophages.

Figure 3.1
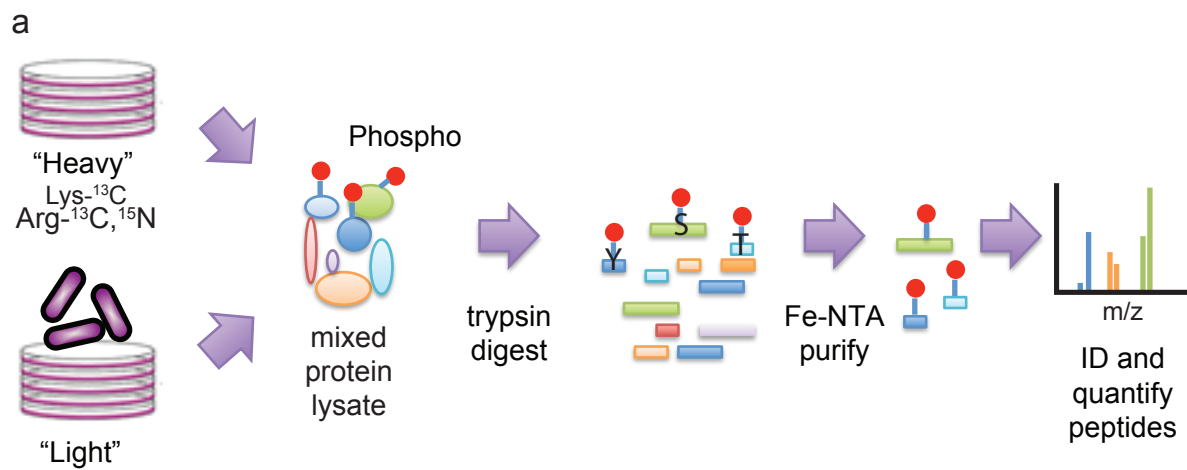
Figure 3.1: Experimental approach to identifying phosphorylation of macrophages during infection.

(A) Schematic of the phospho-peptide affinity enrichment protocol to identify phosphorylated substrates during bacterial infection.

Figure 3.2

TB LM SE

Scale (log$_2$)

3.0 2.0 1.0 0.0 -1.0 -2.0 -3.0
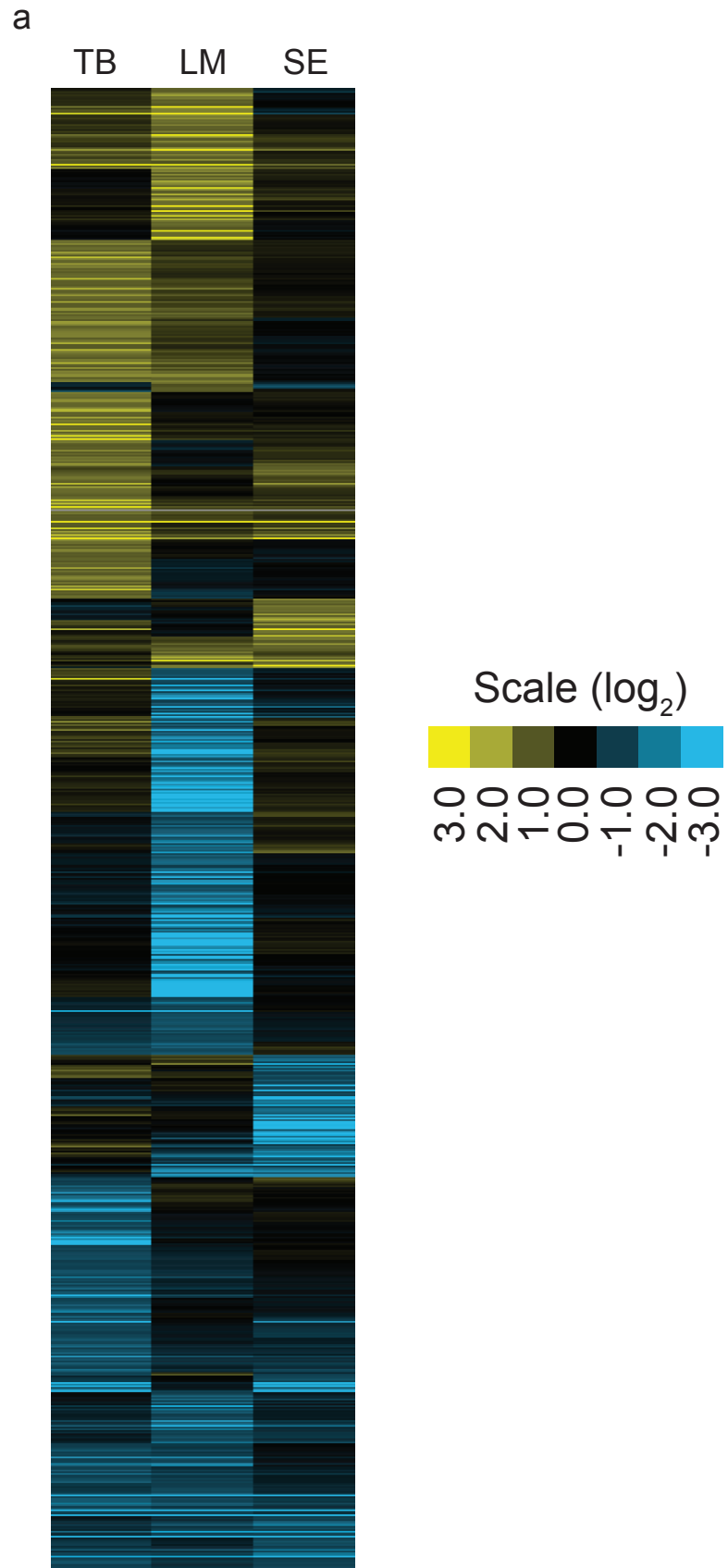
Figure 3.2: Global phosphorylation observed during infection.

(A) Heat map of the average log2 fold change in phosphorylation for each serine, threonine, and

tyrosine site detected in all three bacterial infections that was significant (≥two-fold change

relative to mock infection) in at least one infection.

Figure 3.3

a   b   c

L. monocytogenes   *S. typhimurium*   *M. tuberculosis*

WT   Δ*hly*   WT   Δ*spi1/2*   WT   Δ*esx1*

Scale (log$_2$)

3.0 2.0 1.0 0.0 -1.0 -2.0 -3.0
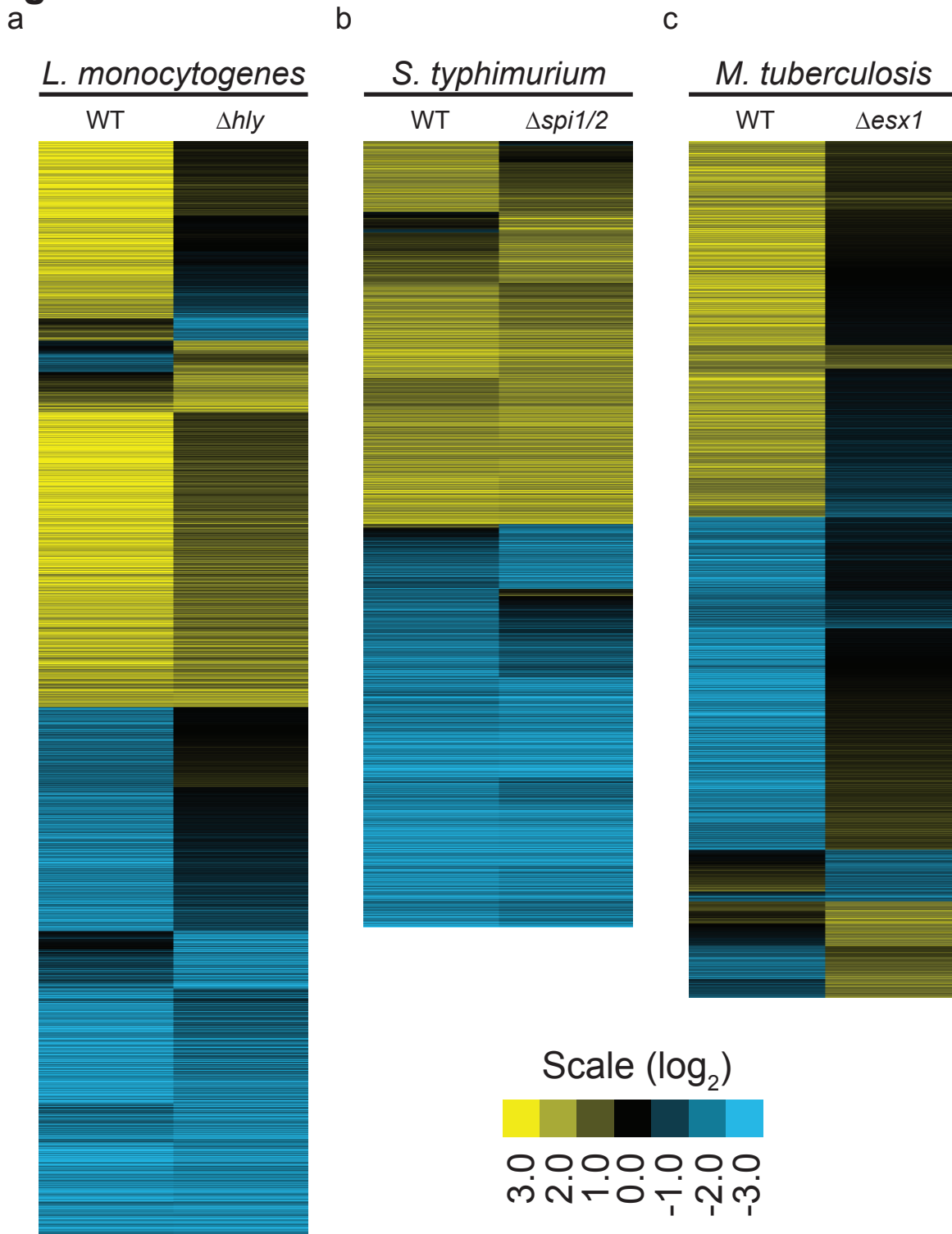
Figure 3.3: Phosphorylation in response to bacterial virulence.

(A) Heat map of the average log2 fold change in phosphorylation for each site detected in wild-type (wt) and ΔHLY *Listeria monocytogenes* infections that was significant (≥two-fold change relative to mock infection) in at least one infection.

(B) Heat map of the average log2 fold change in phosphorylation for each site detected in wild-type (wt) and ΔssAVΔorgA (Δspi1/2) *Salmonella typhimurium* infections that was significant (≥two-fold change relative to mock infection) in at least one infection.

(C) Heat map of the average log2 fold change in phosphorylation for each site detected in wild-type (wt) and ΔEccD (Δesx1) *Mycobacterium tuberculosis* infections that was significant (≥two-fold change relative to mock infection) in at least one infection.

Figure 3.4

a

Figure 3.4: Phosphorylation targets that modify *Mycobacterium tuberculosis* replication in macrophages.

(A) J774 mouse macrophages stably overexpressing GFP, IEX1, or BNIP3L were infected with autoluminescent *Mycobacterium tuberculosis* and luminescence was monitored every 24 hours and values plotted as fold change relative to t=0. All measurements shown as means ± s.e.m. *p<0.05, **p<0.005 by two-tailed Student's t-test.

Figure 3.5
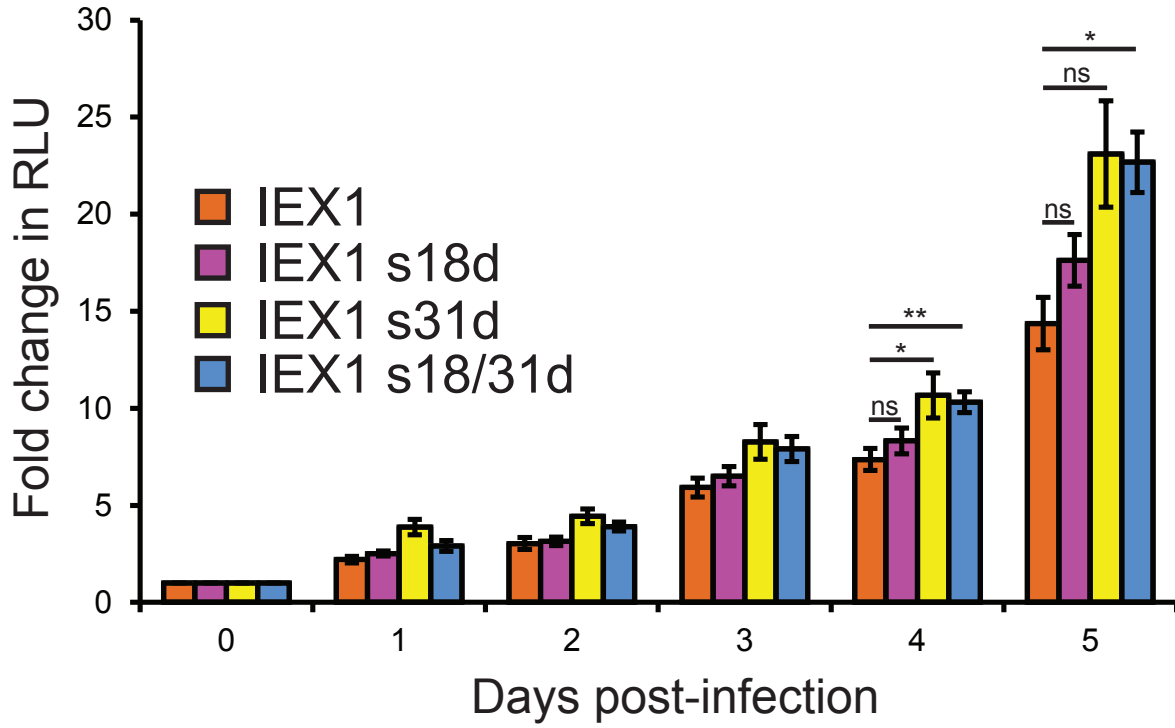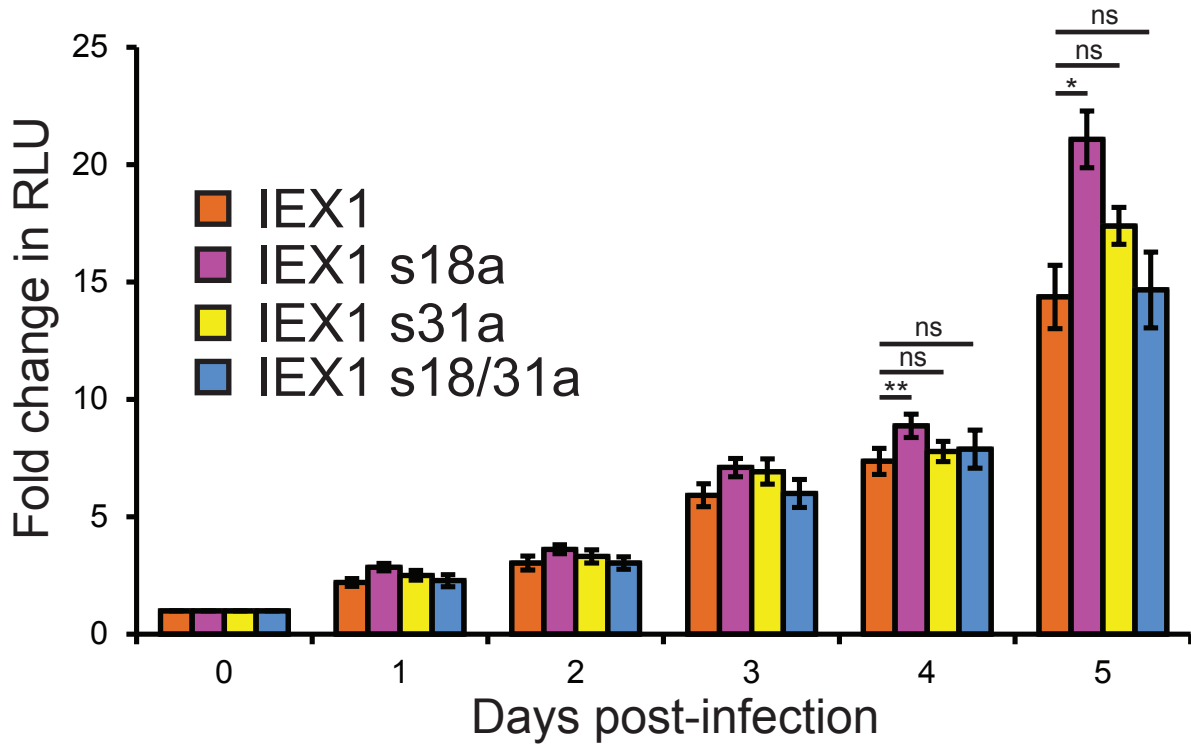
Figure 3.5: Mutational analysis of IEX1 serine phosphorylation during *Mycobacterium tuberculosis* infection in macrophages.

(A) J774 mouse macrophages stably overexpressing wild-type IEX1, or IEX1 harboring serine to aspartic acid mutations, were infected with autoluminescent *Mycobacterium tuberculosis* and luminescence was monitored every 24 hours and values plotted as fold change relative to t=0.

(B) J774 mouse macrophages stably overexpressing wild-type IEX1, or IEX1 harboring serine to alanine mutations, were infected with autoluminescent *Mycobacterium tuberculosis* and luminescence was monitored every 24 hours and values plotted as fold change relative to t=0. All measurements shown as means ± s.e.m. ns=not significant *p<0.05, **p<0.005 by two-tailed Student's t-test.

Figure 3.6

a

b
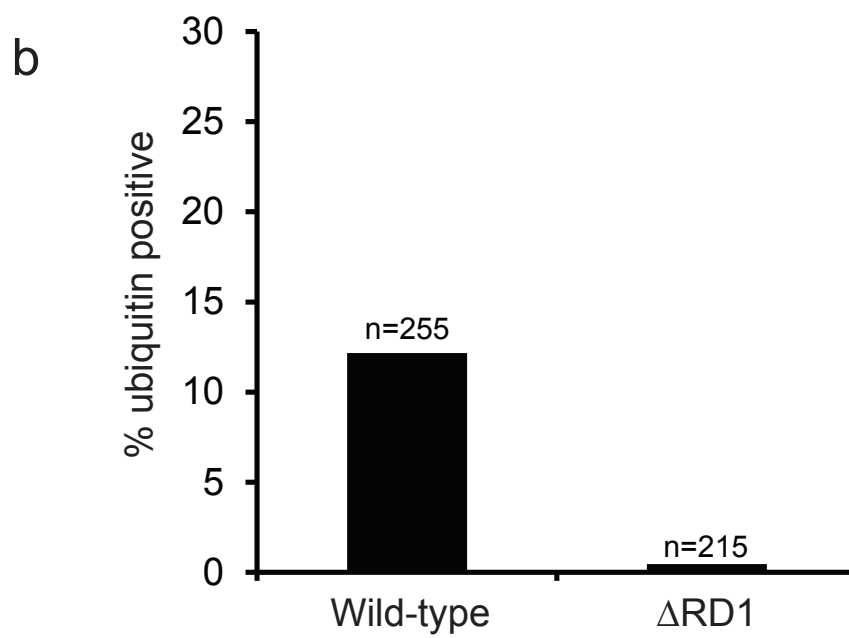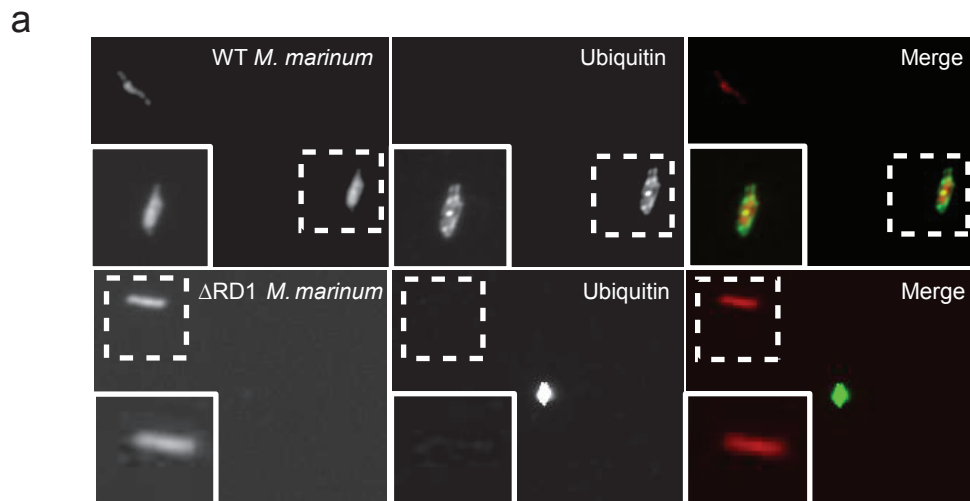
Figure 3.6: *Mycobacterium marinum* **isolated from macrophages remain ubiquitin positive.**

(A) Fluorescence images of mcherry-expressing (red) wild-type or ΔRD1 *Mycobacterium marinum* isolated from bone marrow-derived macrophages after six hours of infection and immunostained with anti-ubiquitin antibody (green).

(B) Quantitative analysis of colocalization with ubiquitin.

Figure 3.7

a
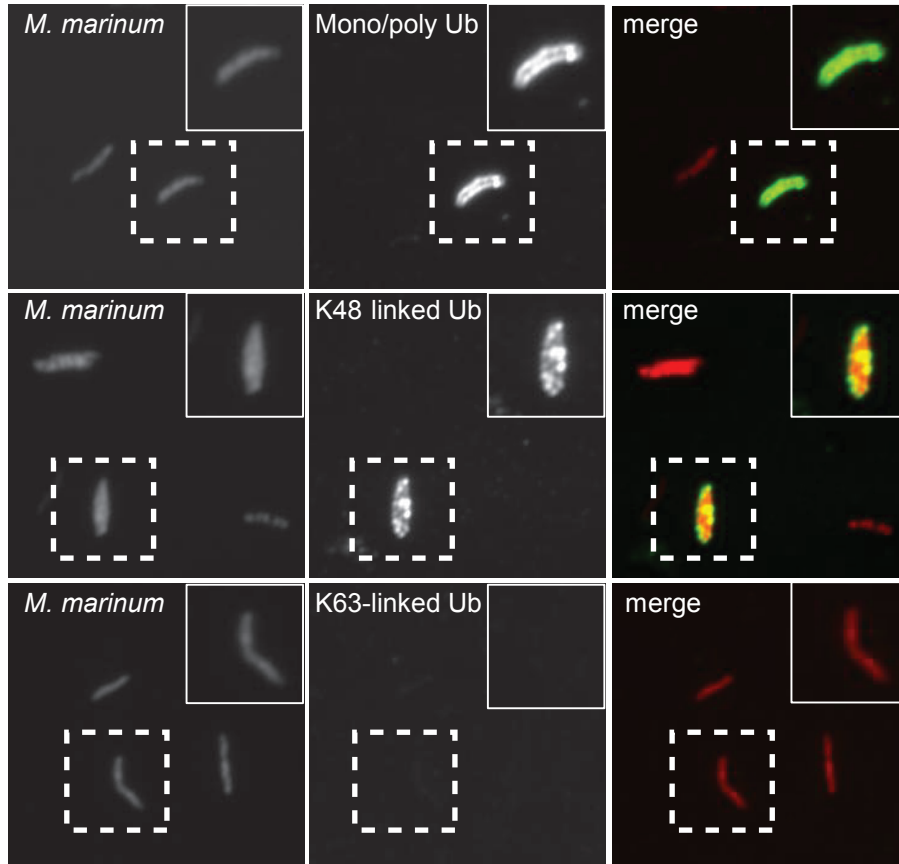
b
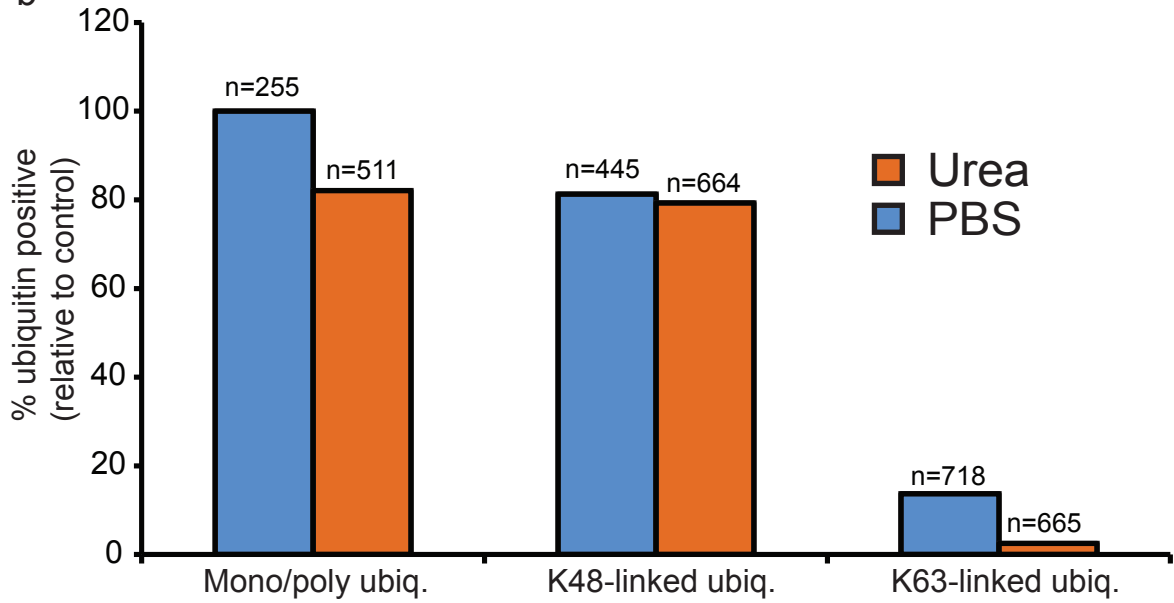
Figure 3.7: Denaturing conditions do not remove K48-linked ubiquitin from

*Mycobacterium marinum***.**

(A) Fluorescence images of mcherry-expressing (red) wild-type *Mycobacterium marinum* isolated from bone marrow-derived macrophages after six hours of infection and immunostained with antibodies recognizing mono/poly, K48-linked, or K63-linked ubiquitin (green).

(B) Quantitative analysis of colocalization with mono/poly, K48-linked, or K63-linked ubiquitin after the bacteria have been washed three times with PBS or 8M urea. Coloclaiztion measured as the percent positive relative to PBS washed bacteria stained with the anti-mono/poly ubiquitin antibody.

Figure 3.8
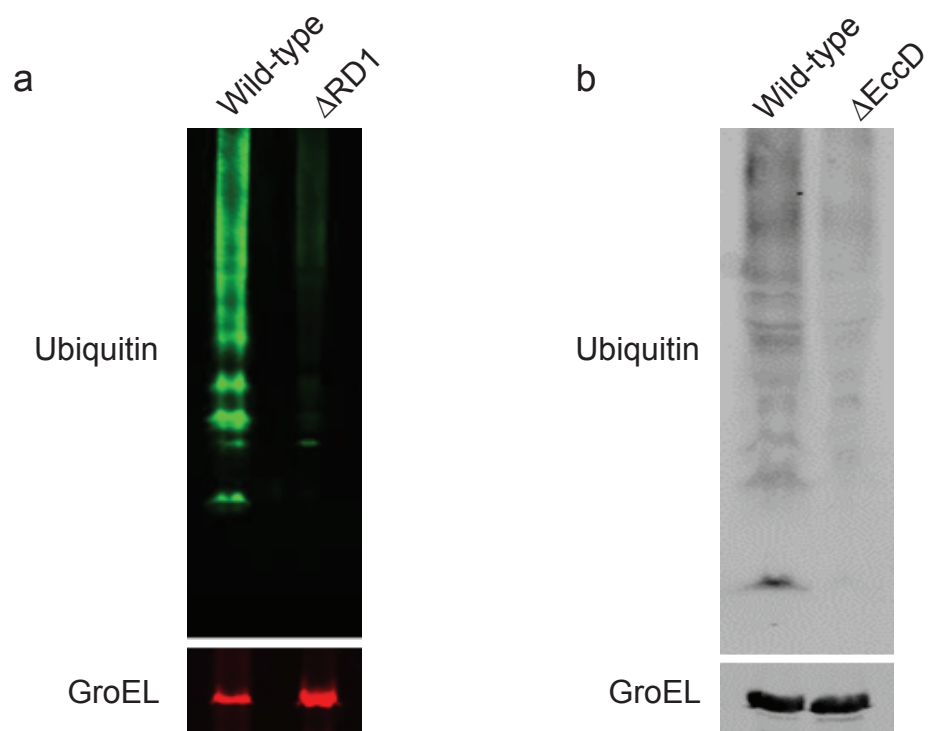
Figure 3.8: Western blot detection of ubiquitylated proteins from isolated bacteria after macrophage infection.

(A) Ubiquitin and GroEL protein levels were determined by western blot from wild-type or ΔRD1 *Mycobacterium marinum* that was washed three times with 8M urea after being isolated from infected RAW264.7 macrophages.

(B) Ubiquitin and GroEL protein levels were determined by western blot from wild-type or ΔEccD *Mycobacterium tuberculosis* that was washed three times with 8M urea after being isolated from infected RAW264.7 macrophages.

Figure 3.9

a
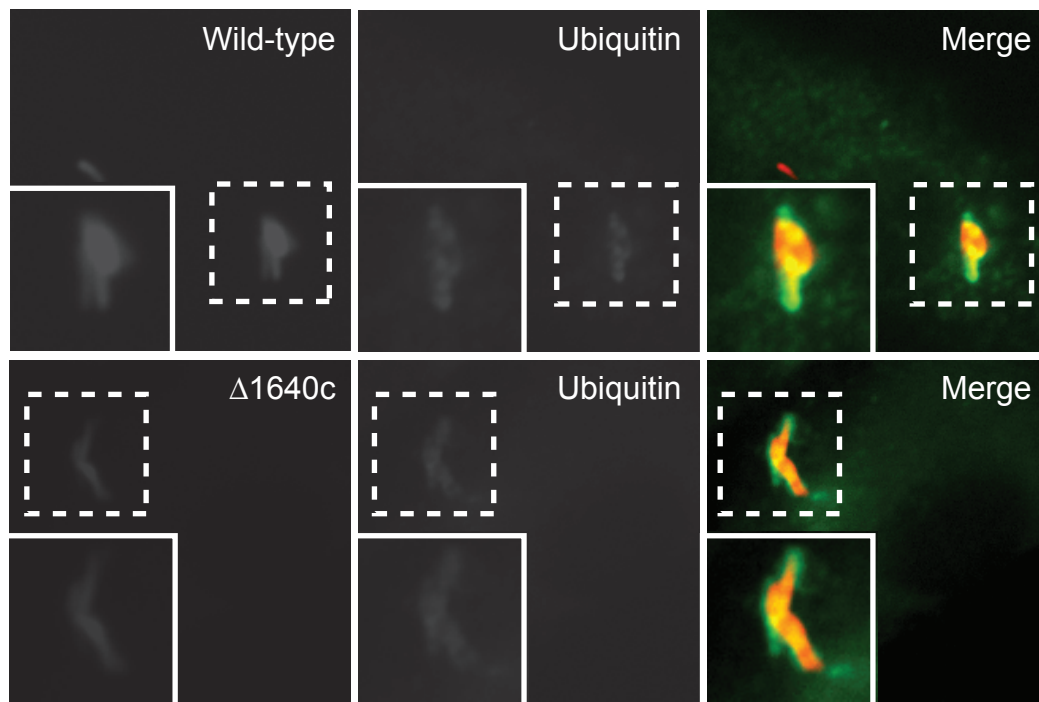
b
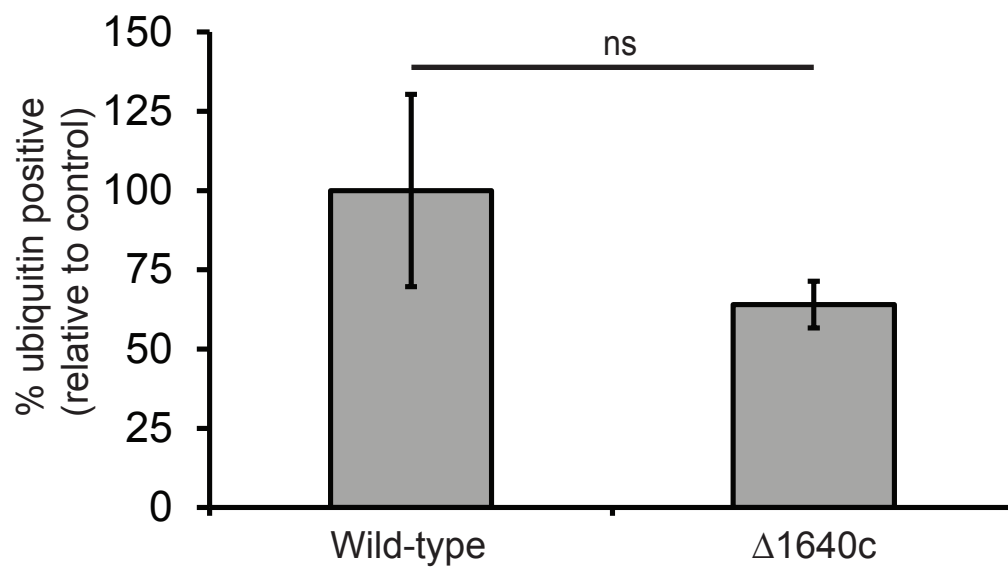
Figure 3.9: Lysinylated-lipid mutant bacteria are ubiquitylated during infection.

(A) Fluorescence images of bone marrow-derived macrophages infected for six hours with mcherry-expressing (red) wild-type or Δ1640c *Mycobacterium tuberculosis* and stained with anti-ubiquitin antibody (green).

(B) Quantitative analysis of colocalization with ubiquitin at six hours post-infection. All measurements shown as means ± s.e.m. ns=not significant by two-tailed Student's t-test.

Chapter 4: Conclusions

Mycobacterium tuberculosis remains the most infectious and deadliest bacterial pathogen. The scientific community has studied *Mycobacterium tuberculosis* for over 100 years and we still are only beginning to understand the complex interaction between the bacteria and its host cell, the macrophage. Ubiquitin has been identified as a fundamental signaling molecule used by the host early during infection to alert the cell that it is infected. While ubiquitin has been known to play a critical role in detection of intracellular pathogens, global ubiquitylation changes in the macrophage during infection have remained a mystery, as facile tools to study this phenomenon have been lacking.

Here we have applied SILAC coupled with di-glycine peptide purification to infected cells, for the first time, to quantitatively measure changes in ubiquitylation of the host proteome during infection with three intracellular bacterial pathogens: *Listeria monocytogenes, Salmonella typhimurium,* and *Mycobacterium tuberculosis*. Due to the conserved transcriptional response to infection by these pathogens, we had expected that the ubiquitylation response would be largely the same during infection with all three pathogens. To our surprise, there was a huge diversity in response to infection with each pathogen; a majority of the changes in ubiquitylation were specific to the infecting bacteria, with few "core" changes. We also used secretion-deficient mutants for each bacterium to define the set of ubiquitylation changes that require pore formation in the phagosome, and effector delivery in to the host.

We have used this information to identify a number of ubiquitylated proteins, through a functional screen, that modify *M. tuberculosis* pathogenicity in its host cell. This screen revealed

OASL1, a translational repressor, as playing a critical role during infection. Overexpression of OASL1 represses translation of the transcription factor IRF7, and *M. tuberculosis* requires IRF7 to be present in the macrophage to replicate normally. We have used RNAseq to identify the transcriptional regulon of IRF7 during *M. tuberculosis* infection, and have identified a number of IRF7 transcriptional targets that contribute to bacterial pathogenesis. We have also shown that this pathway is critical not only in cultured cells, but *in vivo* through aerosol challenge of wild-type and *Irf7*$^{-/-}$ knockout mice. This work represents one of thousands of proteins whose ubiquitylation levels change in macrophages during infection, and there are undoubtedly many others represented in our dataset that contribute to pathogenesis and host defense to intracellular bacterial pathogens.

We have applied this same global approach to measure changes in the phosphoproteome of infected macrophages with these three pathogens. We see increased conservation of phosphorylation changes in the macrophage proteome relative to the ubiquitylation analysis we had done previously. We have also used our secretion mutants to define phosphorylation that requires bacterial interaction with the host cytoplasm. We used this analysis to direct a second screen of proteins that contribute to bacterial virulence, identifying IEX1 as a protein critical for bacterial growth. While IEX1 is dephosphorylated at two sites during infection, mutational analysis has identified dephosphorylation of one residue, serine 31, as likely being important for the macrophage response to infection. The phosphoproteomics described here will be used to guide future studies of how *M. tuberculosis* infection drives macrophage proteome phosphorylation, and the contribution of the ESX-1 secretion system to this process.

Chapter 5: Methods

Mice and macrophages

Irf7^{-/-} knockout mice on the C57BL/6 background were a gift from T. Taniguchi (University of Tokyo). Wild-type C57BL/6 mice were purchased from Jackson Laboratories. Bone marrow-derived macrophages were isolated from mouse femurs as described previously[14] and cultured in DMEM H-21 supplemented with 20% FBS and 10% MCSF derived from 3T3-MCSF cells. J774 and RAW264.7 cells were obtained from ATCC.

Plasmids, antibodies, and western blotting

pENTR1A no ccDB (w48-1) was a gift from Eric Campeau (Addgene plasmid # 17398). pLenti CMV Puro DEST (w118-1) was a gift from Eric Campeau (Addgene plasmid # 17452). pLenti CMV Blast DEST (706-1) was a gift from Eric Campeau (Addgene plasmid # 17451). pMD2.G was a gift from Didier Trono (Addgene plasmid # 12259). psPAX2 was a gift from Didier Trono (Addgene plasmid # 12260) shRNA constructs were cloned into the Mission pLKO.1 lentivirus system from Sigma. The following antibodies were used: OasL1 (Abcam ab116220), Actin (Abcam ab6276), Irf7 (Abcam ab109255), mono/poly ubiquitin (Millipore 04-263), K48-linked ubiquitin (Millipore 05-1307), K63-linked ubiquitin (Millipore 05-1308), FLAG (Sigma F1804), GroEL (Assay Designs sps-875), Streptavidin-800 (Li-Cor 92532230) and ATP6E (Santa Cruz #20946). Protein lysates from cells were obtained by lysing in 2% Triton X-100, 150 mM NaCl, 50 mM Tris pH 7.4 and protease inhibitor cocktail tablets (Roche #04693124001). Lysates were electrophoresed on 4-20% Tris-HCL gels (Bio-Rad #456-1083), transferred to nitrocellulose

membranes, and analyzed on an Odyssey Imager (Li-Cor) according to the manufacturer's instructions.

Bacterial strains

The following bacterial strains were used: wild-type and ΔRD1 *M. marinum* (M strain), wild-type and Δ*eccD M. tuberculosis* (Erdman) were a gift from O. Rosenberg (UC San Francisco), wild-type Δ1640c *M. tuberculosis* (H37rv) were a gift from S. Stanley (UC Berkeley), wild-type and Δ*hly L. monocytogenes* (10403s) were a gift from D. Portnoy (UC Berkeley), and wild-type and Δ*ssAV*Δ*orgA S. typhimurium* (SL1344) were a gift from D. Monack (Stanford).

Macrophage infections with luminescent *M. tuberculosis*

Cultures of *M. tuberculosis* expressing a codon-optimized *luxBCADE* operon were washed twice with PBS, sonicated to disperse clumps, and diluted into DMEM supplemented with 10% horse serum. Media was removed from the macrophages, monolayers were overlaid with the bacterial suspension at an m.o.i of one, and centrifuged for 10 minutes at 411g. After centrifugation, the monolayers were washed twice with PBS, bacterial luminescence was read with a one second integration time on a Tecan Infinite 200 microplate reader, and media was returned to the plate. At 24 hour intervals, media was removed from the infected cells, and bacterial luminescence was determined.

Immunofluorescence and Griess assay

Infected cells were immunostained as described previously[14] and images were acquired using a Yokogawa CSU22 Spinning Disk Confocal (Solamere Technology Group) on a Nikon TE2000U inverted microscope. Briefly, macrophages were seeded onto poly-lysine coated coverslips and

infected with mcherry-expressing wild-type *M. tuberculosis*. Cells were infected at an m.o.i. of one, and fixed in 4% paraformaldehyde for 20 minutes at the indicated time points. Cells were incubated with the indicated primary antibodies for 3 h at room temperature in 5% milk, 0.05% saponin, and visualized using secondary Alexa-fluor488 antibodies. Colocalization studies were performed as blinded experiments, with a minimum count of 100 cells per coverslip and performed in triplicate. The Griess assay was performed as described previously (Stich et al. 1998) with the following differences: 100 µL of macrophage supernatant was used in the assay, and the cells were grown in phenol red-free media.

Mouse infections

Female (10-13 weeks old) mice were infected with *M. tuberculosis* via a low-dose aerosol infection (250 c.f.u) as described previously (Ohol et al. 2010). Lungs, liver, and spleens were collected at the indicated time points, homogenized, and dilutions were plated on 7H10 agar plates. For time to death experiments, male (10-13 weeks old) mice were infected with *M. tuberculosis* via a low-dose aerosol infection (165 c.f.u) as described previously (Ohol et al. 2010). Time to death was determined when the infected mice lost 15% of their maximal body weight, as per UC San Francisco IACUC protocols.

Bacterial isolation from infected macrophages

Bacteria (*M. marinum* or *M. tuberculosis)* were infected into macrophages as described above. At six hours post-infection, the cells were washed once with PBS, scraped in PBS, and pelleted. Cells were resuspended in 1% NP40, 150 mM NaCl, 50 mM Tris pH 7.4, and protease inhibitor cocktail tablets (Roche #04693124001), incubated for five minutes at room temperature, and cellular debris was pelleted at 300xg for 5 minutes. Bacteria were then pelleted at 7500xg, and the pellets were washed three times with PBS (or 8M urea in PBS). Pellets were then

resuspended in PBS + 0.05% Tween 80 and spun on to poly-lysine treated cover slips and stained for immunofluorescence as described above. Alternatively, pellets were resuspended in 150 mM NaCl, 50 mM Tris pH 7.4, and 0.1% Rapigest (Waters 186001860) and sonicated (Sonics and Materials Inc. model VC 130) for 15 minutes (one minute on, 30 second off cycles on high). Lysates were then ready for western blot detection or submission for mass spectrometry.

Lentiviral overexpression and knockdown

ORFs were cloned into the pENTR1A construct and transferred into the pLENTI CMV puro or blast vectors using a Gateway enzyme mix (Invitrogen #56484). Lentivirus was produced by co-transfection of the pLenti CMV plasmids with pMD2.G and psPAX2 plasmids using Polyjet (Signagen Laboratories Sl100688) according to manufacturer's instructions. Lentivirus expressing shRNAs targeting mouse Irf7 transcripts (Irf7 shRNA1 was Sigma TRCN0000077292 and Irf7 shRNA2 was Sigma TRCN0000077289) were generated using the Mission PLKO.1 lentivirus system from Sigma. Lentivirus expressing shRNAs targeting mouse OasL1 transcripts (OasL1 shRNA1 was Sigma TRCN0000075898 and OasL1 shRNA2 was Sigma TRCN0000075902) were generated using the Mission PLKO.1 lentivirus system from Sigma. A lentivirus expressing a scrambled, non-targeting shRNA was used as a control. J774 cells were transduced and selected on Puromycin (2 μg/mL) or Blasticidin (0.75 μg/mL).

RNA isolation, qPCR, and RNAseq

RNA was isolated and purified from cells using TRIzol and the PureLink RNA Mini Kit (Life Technologies #15596 and #12183018A) according to manufacturer's instructions. One μg of RNA was reverse transcribed using the First Strand cDNA Synthesis Kit (Life Technologies

K1681) according to manufacturer's instructions and qPCR analysis was performed in triplicate

using a Bio Rad CFX96 Real-Time PCR detection system. The sequences for qPCR primer (5' to

3') were: *Irf7* forward (AGCCACGGAAAATAGGGAAG) and reverse

(GCATCACTAGAAAGCAGAGGG), *OasL1* forward (GAAGGCTACAGATGGGACATAG)

and reverse (GATATCGGGTGCTCTCTTCAC), and *Actin* forward

(GGTGTGATGGTGGGAATGG) and reverse (GCCCTCGTCACCCACATAGGA). For

RNAseq sample preparation, 5 µg of RNA was used as the input for the reactions, and the exact

protocol can be found in Wang et al. 2011 as a downloadable PDF file (File s1). Reagents were

proved by Eric Chow in the UCSF Center for Advanced Technology.

SILAC labelling and di-glycine peptide sample preparation

RAW264.7 cells were labelled for 15 days in SILAC DMEM (Thermo Scientific #89985)

supplemented with heavy or light labeled arginine (Thermo Scientific #89989 and #89990),

heavy or light labeled lysine (Thermo Scientific #89987 and #89988), 10% dialyzed FBS

(Thermo Scientific #88212), and 20 mM HEPES buffer. Mock and bacterial infections (m.o.i of

10) were carried out in the described SILAC media supplemented with 10% dialyzed horse

serum. At the indicated time points, cells were fixed for 10 minutes in 100% methanol and then

washed three times with PBS. Cells were lysed in 8M urea, 150 mM NaCl, 100 mM Tris pH 8.0

and protease inhibitor cocktail tablets (Roche #04693124001), sonicated two times at seven

watts (Sonics and Materials Inc. model VC 130), and protein concentrations were measured

using a micro BCA kit (Thermo #23235). Five mg of light-labeled lysate was mixed with five

mg of heavy-labeled lysate, and the mixture was treated with 5 mM TCEP for 20 minutes at

60ºC, chilled on ice for 10 minutes, then treated with 10 mM iodoacetamide at 25ºC for 15

minutes in the dark. Lysates were then diluted to 2M urea with 100 mM Tris pH 8.0 prior to

trypsin digestion, and 100 µg trypsin (Promega v5280) was added and incubated for 16 hours at 25ºC. Peptides were purified over a c18 column (Waters Wat023590) according to manufacturer's instructions and lyophilized for 48 hours.

Immunoprecipitation of di-glycine peptides

Lyophilized peptides were resuspended in 1 mL IAP buffer (50 mM MOPS (pH 7.4), 10 mM Na_2HPO_4, 50 mM NaCl) and sonicated for 30 minutes at 4ºC (Diagenode Bioruptor). Anti-di-glycine peptide beads (Cell Signaling #5562) were washed twice with IAP buffer, and incubated with resuspended peptides for 90 minutes at 4ºC. Beads were washed three times with IAP buffer, twice with water, and eluted with 0.15% trifluoro acetic acid. The eluted peptides were then desalted using the Stage-tip method and the samples were dried.

Affinity capture of phosphor-peptides

Ni-NTA beads were placed in an empty vacuum column and washed with 100 mM EDTA for 1 minute and water for one minute (repeated 3 times) to strip away the nickel. Beads were incubated with 3 times with 15 mM $FeCl_3$ for 1 minute, washed with 3 times for one minute to generate Fe-NTA beads. Beads were washed once with 0.5% formic acid (FA) and aliquoted. 1 mg lyophilized peptides (prepared as described above in "SILAC labelling and di-glycine peptide sample preparation") was dissolved in 50% acetonitrile (ACN) 0.25% trifluoro acetic acid (TFA), and once dissolved, brought to 80% CAN 0.1% TFA and added to Fe-NTA beads for 1-2 minutes, pipetted up and down, and incubated a further 1-2 minutes. Beads were then washed four times with 80% CAN 0.1% TFA, two times with 0.5% FA, and eluted in 500 mM phosphate for 1-2 minutes (repeated elution once). Samples were desalted and dried as described above.

Data analysis

Heat maps were generated using Cluster 3.0 (Eisen and Hoon, 2002) and Java Treeview (Saldanha, 2004). RNAseq analysis was performed using the TopHat2 suite of products (Kim et al. 2013).

Statistics

Two-tailed unpaired Student's t-tests were used for the analysis of bacterial luminescence and mouse c.f.u. assays. A log-rank test was used for the analysis of mouse survival. Statistical analysis of the combined set of biological replicates was performed using a computational pipeline built around the MSstats package. Briefly, after median-centering the log2-scaled intensity distributions across all replicates, a mixed or fixed effect model was fitted for every protein or modification site to account for systematic sources of variation when computing the significance test. Adjustments were made for all test results for multiple testing by applying a Benjamini-Hochberg correction on the resulting p-values and applying a composite threshold ($p < 0.05$ and log2-fold-change > 1 or < -1) to determine the set of significantly changing proteins or lysine sites.

Datasets

All data sets saved as excel files in the Cox lab drop box folder as well as on Jeff's computer. RNAseq data was averaged data from two biological replicates. The data is saved as excel files of the Cuffdiff output of: Uninfected vs. 24 hour infected wild-type bone marrow-derived macrophages at an MOI of one (saved as WTunvs24), Uninfected vs. 72 hour infected wild-type bone marrow-derived macrophages at an MOI of one (saved as WTunvs72), Uninfected vs. 24 hour infected Irf7 knockout bone marrow-derived macrophages at an MOI of

one (saved as IRFunvs24), Uninfected vs. 72 hour infected Irf7 knockout bone marrow-derived

macrophages at an MOI of one (saved as IRFunvs72). I also performed the direct comparison of

each time point: Uninfected wild-type vs. uninfected Irf7 knockout bone marrow-derived

macrophages (saved as WTvsIRFuninf), 24 hour infected wild-type vs. 24 hour infected IRF7

knockout bone marrow-derived macrophages (saved as WTvsIRF24), and 72 hour infected wild-

type vs. 72 hour infected IRF7 knockout bone marrow-derived macrophages (saved as

WTvsIRF72). All of the UbiScan data is merged into one large file that contains information for

every site detected for every infection we did (called TP_UbiScan). This file contains log2 fold

change and p values for every unique, ubiquitylated lysine residue as well as log2 fold change

and p values for all lysine residues averaged across each protein. All of the phosphoproteomics

data for the three wild-type bacteria is saved in one large file (called

TP_Phosphorylation_WTbugs). The phosphoproteomics data for wild-type versus secretion

deficient bugs is saved in one file with three separate tabs, one for each species for bacteria

(saved as TP_Phosphorylation_secretion). This data has only been analyzed using MaxQuant

(not MS Stats which is our newer version of statistical analysis) so we only have the data as fold

change in each individual experiment instead of averaged between two biological replicates, and

the data is all in log10 not log2 like the UbiScan and RNAseq data.

Table 1: Total number of proteins and enrichment score for funtional clusters of significantly ubiquitylated proteins during *M. tuberculosis* infection.

Functional clusters:	# of Proteins:	Enrichment Score:
Mitochondria	68	13.59
Cell Death	29	4.66
Protein trafficking	49	4.57
Nucelotide metabolism	16	3.9
Lysosome	13	3.68
Reduction-Oxidation	28	2.33
Innate immunity	33	2.25
Chromatin	15	2.01
Other	42	NA

Table 2: Total number of proteins and enrichment score for funtional clusters of significantly ubiquitylated proteins during *L. monocytogenes* infection.

Functional clusters:	# of Proteins:	Enrichment Score:
Cell Death	33	5.66
ER	41	5.6
Translation	34	3.58
DNA repair	24	3.35
Protein trafficking	59	3.2
Lipid biosynthesis	29	3.2
Chromatin	35	3.14
Catepolic processes	28	2.72
Nucelotide metabolism	20	2.45
Other	39	NA

Table 3: Total number of proteins and enrichment score for funtional clusters of significantly ubiquitylated proteins during *S. typhimurium* infection.

Functional clusters:	# of Proteins:	Enrichment Score:
Chromatin	17	4.96
Protein trafficking	8	2.28
Nucelotide metabolism	4	2.05
Other	10	NA

Table 4: Results from screened ubiquitylated proteins.

Gene name:	Effect on M.tb growth	Effect on macrophage survival:
APOL9A	None	None
ARL8B	None	None
BNIP1	Increased growth	None
CD14	None	Decreased survival
CXCL2	None	None
DET1	None	None
DHRS1	Increased growth	None
DTX3L	None	None
GAL8	None	None
GPR84	None	None
GRN	None	None
GRP162	None	None
LAPTM5	Increased growth	None
LMBRD2	None	None
LRSAM1	None	None
MPEG1	None	None
OASL1	Decreased growth	Increased survival
ORD4	None	None
PELLINO1	Decreased growth	Increased survival
PLBD1	None	None
PLK2	None	None
REEP4	None	None
RENR	None	None
RIPK2	None	None
RNF141	None	None
RNF150	None	None
RNF169	None	None
RNF216	None	None
SOCS3	None	None
STUB1	None	None
TAX1BP1	None	None
TNIP1	None	None
TNIP2	Increased growth	None
TRAF6	None	None
TRIM25	None	None
UBE2C	None	None
VAMP8	Increased growth	None
VAT1	None	None
ZDHHC20	None	Decreased survival

Table 5: List of genes regulated by IRF7 during infection.

Gene name:	WT/ΔIRF7, log2:
Acaa1b	-100
Acpp	4.36546
Acta2	4.3843
Aen,Isg20	2.03647
Atp6v0d2	-1.53066
Axl	2.34513
Cav1	2.22222
Ccl5	1.75213
Ccnb2	-2.60242
Cd74,Mir5107	2.27488
Cdca2	-2.05598
Cmpk2	1.49412
Col1a1	4.73484
Col4a2	3.15124
Cxcl10	2.17891
Dmpk	1.78769
Dst	1.43245
Ednrb	-1.5391
Fn1	1.64666
Gbp1,Gbp2	1.42386
Gbp5	1.43656
Gm14446	3.05096
Gm21949,Iqcj,Schip1	100
Gm4951	3.02942
Gm5150	1.76377
H2-M2	1.63141
Hebp1	-1.83401
Helz2	1.33746
Hipk3,Mir1902	3.03201
I830012O16Rik	1.93739
Id3	1.60567
Ifi205	2.17664
Ifi44	2.98465
Ifit3	1.4413
Iigp1	3.35164

Gene name:	WT/ΔIRF7, log2:
Iqgap3	-1.53359
Irf7	9.50972
Isg15	1.38808
Itgb7	1.61324
Lox	1.96031
Ly6a	2.89177
Map4k1	-2.67354
Met	1.98427
Mir3082,Stub1	4.18959
Mir5114,Scd2,Scd3	-2.48498
Mmp13	1.38151
Mmp14	1.35828
Mx1	1.7155
Nav1	-9.17567
Oasl1	2.24935
Olfml3	1.8324
Plekhn1	1.40313
Ptges	1.80525
Ptgs2	1.38392
Pydc3	1.72462
Scarf1	1.77268
Sdc1	1.3619
Serpinb2	3.48278
Serpine1	3.52423
Slamf9	1.28616
Slc13a3	1.98242
Slc26a7	-100
Slc35g2	100
Slc7a2	1.28846
Slco3a1	1.85643
Slfn1	1.35629
Top2a	-1.65513
Uchl1	4.19801
Usp18	1.23508

References:

Angot et al. PLoS Pathog. 2007 Jan; 3(1):e3.

Baba et al. J Cell Biol. 1994 Mar; 124(6):903-13.

Birmingham et al. J Biol Chem. 2006 Apr 21; 281(16):11374-83.

Blanchette et al. Immunology. 2003 Apr; 108(4):513-22.

Bohsali et al. BMC Microbiol. 2010 Sep 10; 10:237.

Cemma et al. Autophagy. 2011 Mar; 7(3):341-5.

Collins et al. PLoS Pathog. 2009 May; 5(5):e1000430.

Daffis et al. J Virol. 2008 Sep; 82(17):8465-75.

Daqvadori et al. Immunity. 2015 Apr 21;42(4):640-53.

Davis and Gack. Virology. 2015 May; 479-480:52-65.

Eaisen and Hoon. 2001; Cluster 3.0 Manual.

Furuno et al. J Biochem. 1982 Jun; 91(6):1943-50.

Getahun et al. Clin Infect Dis. 2010 May 15; 50 Suppl 3:S201-7.

Glomski et al. Infect Immun. 2003 Dec; 71(12): 6754–6765.

Gutierrez et al. Cell. 2004 Dec 17; 119(6):753-66.

Huang et al. Science. 2001 Oct 26; 294(5543):870-5.

Huang et al. Nat Protoc. 2009; 4(1):44-57.

Imami et al. Molecular & Cellular Proteomics. 2013; 12(6):1632-1643.

Ivanov and Roy. Nat Immunol. 2013 Dec;14 (12):1219-28.

Iwasaki and Medzhitov. Nat Immunol. 2015 Apr; 16(4):343-53.

Jager et al. Nature. 2011 Dec 21; 481(7381):371-5.

Janeway and Medzhitov. Annu Rev Immunol. 2002; 20: 197-216.

Kampmann et al. J Infect Dis. 2000 Sep;182(3):895-901.

Kauffmann. <u>Nat Rev Immunol.</u> 2001 Oct; 1(1):20-30.

Kebaya et al. <u>EMBO J.</u> 2000 Nov 1;19(21):5720-8.

Kim et al. <u>Mol Cell.</u> 2011 Oct 21; 44 (2):325-40.

Kim et al. <u>Genome Biol.</u> 2013 Apr 25; 14(4):R36. doi: 10.1186/gb-2013-14-4-r36.

Krachler et al. <u>J Cell Biol.</u> 2011 Dec 26; 195(7):1083-92.

Kwon. <u>J Korean Med Sci.</u> 1997 Dec; 12(6):481-7.

Lam et al. <u>Autophagy.</u> 2013 Jul;9(7):985-95.

Lambert et al. <u>J Proteomics.</u> 2015 Apr 6; 118:81-94.

Leber et al. <u>PLoS Pathog.</u> 2008 Jan; 4(1):e6.

Lee et al. <u>EMBO J.</u> 2010 Mar 3; 29(5):969-80.

Lee et al. <u>Nat Immunol.</u> 2013 Apr;14(4):346-55.

Lerena and Colombo. <u>Cell Microbiol.</u> 2011 Jun; 13(6):814-35.

Macgurn and Cox. <u>Infect Immun.</u> 2007 Jun; 75(6):2668-78.

Macmicking et al. <u>Proc Natl Acad Sci U S A.</u> 1997 May 13;94(10):5243-8.

Maloney et al. <u>PLoS Pathog.</u> 2009 Jul ;5(7):e1000534.

Manzanillo et al. <u>Cell Host Microbe.</u> 2012 May 17; 11(5):469-80.

Manzanillo et al. <u>Nature.</u> 2013 Sep 26; 501(7468):512-6.

Mesquita et al. <u>PLoS Pathog.</u> 2012;8(6):e1002743.

Miranda et al. <u>Clin Dev Immunol.</u> 2012; 2012:139127.

Mogenson. <u>Clin Microbiol Rev</u>. 2009 Apr; 22(2): 240–273.

Murphy et al. <u>J Biol Chem.</u> 2015 Jun 16.

Narayanan and Edelmann. <u>Front Immunol.</u> 2014 Nov 25; 5:558.

Narendra et al. <u>J Cell Biol.</u> 2008 Dec 1; 183(5):795-803.

Ohol et al. <u>Cell host & microbe</u>. 2010; 7(3):210-220.

Ordureau et al. <u>Mol Cell.</u> 2015 May 21; 58(4):660-676.

Olzmann et al. <u>J Cell Biol.</u> 2007 Sep 10; 178(6):1025-38.

Oshita et al. <u>J Biochem.</u> 1986 Sep; 100(3):623-32.

Pawlowski et al. <u>PLoS Pathog.</u> 2012 Feb; 8(2):e1002464.

Perrin et al. <u>Curr Biol.</u> 2004 May 4; 14(9):806-11.

Ponpuak et al. <u>Immunity.</u> 2010 Mar 26; 32(3):329-41.

Randow et al. <u>Science.</u> 2013 May 10; 340(6133):701-6.

Ribet and Cossart. <u>FEBS Lett.</u> 2010 Jul 2; 584(13):2748-58.

Riley et al. <u>Am J Epidemiol.</u> 1995 Jul 1; 142(1):3-14.

Rodgers et al. <u>Sci Signal.</u> 2011 Sep 20; 4(191):rs9.

Russell. <u>Nat Rev Mol Cell Biol.</u> 2001 Aug; 2(8):569-77.

Sadek et al. <u>Am J Respir Cell Mol Biol.</u> 1998 Sep; 19(3):513-21.

Saldanha. <u>Bioinformatics.</u> 2004 Nov 22; 20(17):3246-8.

Sarraf et al. <u>Nature.</u> 2013 Apr 18; 496(7445):372-6.

Schiebler et al. <u>EMBO Mol Med.</u> 2014 Dec 22;7(2):127-39.

Schmutz et al. <u>Molecular & Cellular Proteomics</u>. 2013; 12(10):2952-2968.

Sha et al. <u>Hum Mol Genet.</u> 2010 Jan 15; 19(2):352-63.

Sivick et al. <u>Cell Host Microbe.</u> 2014 Feb 12;15 (2):203-13.

Stanley et al. <u>Proc Natl Acad Sci U S A.</u> 2003 Oct 28; 100(22):13001-6.

Stich et al. <u>Infect Immun.</u> 1998 Sep; 66(9): 4130–4136.

Teles et al. <u>Science.</u> 2013 Mar 22; 339(6126):1448-53.

Thedieck et al. <u>Mol Microbiol.</u> 2006 Dec; 62(5):1325-39.

Thurston et al. <u>Nat Immunol.</u> 2009 Nov; 10(11):1215-21.

Thurston et al. <u>Nature.</u> 2012 Jan 15; 482(7385):414-8.

Trost et al. <u>Immunity.</u> 2009 Jan 16; 30(1):143-54.

Udeshi et al. <u>Nat Protoc.</u> 2013 Oct; 8(10):1950-60.

UNAIDS. 2014; Fact sheet 2014, Global Statistics

Vance et al. <u>Cell Host Microbe.</u> 2009 Jul 23; 6(1): 10–21.

Vandal et al. <u>Nat Med.</u> 2008 Aug; 14(8):849-54.

Vergne et al. <u>Traffic.</u> 2003 Sep; 4(9):600-6.

Vergne et al. <u>Proc Natl Acad Sci U S A.</u> 2005 Mar 15; 102(11):4033-8.

Wang et al. <u>PLoS One.</u> 2011; 6(10):e26426.

Wang et al. <u>Am J Physiol Endocrinol Metab.</u> 2013 Aug 15; 305(4):E485-95.

Watson et al. <u>Cell.</u> 2012 Aug 17; 150(4):803-15.

Watson et al. <u>Cell Host Microbe.</u> 2015 Jun 10; 17(6):811-9.

World Health Organization. 2014; WHO Global tuberculosis report 2014.

Yang et al. <u>Protein & Cell</u>. 2015;6(4):265-274.

Zheng et al. <u>J Immunol.</u> 2009 Nov 1; 183(9):5909-16.

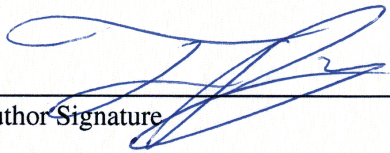Zinngrebe et al. <u>EMBO Rep.</u> 2014 Jan; 15(1):28-45.

Publishing Agreement

It is the policy of the University to encourage the distribution of all theses, dissertations, and manuscripts. Copies of all UCSF theses, dissertations, and manuscripts will be routed to the library via the Graduate Division. The library will make all theses, dissertations, and manuscripts accessible to the public and will preserve these to the best of their abilities, in perpetuity.

__Please sign the following statement:__
I hereby grant permission to the Graduate Division of the University of California, San Francisco to release copies of my thesis, dissertation, or manuscript to the Campus Library to provide access and preservation, in whole or in part, in perpetuity.

_____   7/20/15
Author Signature   Date